TEC-3

Geothermal Energy in the Pacific Region

L. T. Grose and G. V. Keller

May 1975

Appendix A: Exploration for a Geothermal System in the Lualualei Valley, Oahu, Hawaii

M. Tahsin Tasci

Appendix B: Exploration on Adak Island, Alaska

D. L. Butler and G. V. Keller

This project has been supported by the Office of Naval Research, Contract Number N00014-71-A-0430-0004

APPENDIX A

EXPLORATION FOR A GEOTHERMAL SYSTEM IN THE LUALUALEI VALLEY, OAHU, HAWAII

by

M. Tahsin Tasci

Appendix A accompanies a report entitled "Geothermal Energy in the Pacific Region" by L. T. Grose and G. V. Keller, May, 1975. This project has been supported by the Office of Naval Research Contract Number N00014-71-A-0430-0004.

ABSTRACT

Lualualei Naval Magazine is located in the northeastern corner of the Lualualei Valley, Oahu, Hawaii. It has an area of approximately 12 square miles (between latitudes 21°29' and 21°24'25" north and between longitudes 158°09' and 158°05'45" west), with an elevation of about 250 feet above sea level. Shear cliffs of the Waianae Range bound the area to the north, east and south, and alluvial plans of the Lualualei Valley extend all the way to the Pacific Ocean to the west. During late 1974, studies were carried out to determine the geothermal potential. Anomalously low values of electrical resistivities were mapped in the southwest part of the area. In addition, shallow (1 meter) temperature measurements showed that the area with anomalous resistivities was characterized by a temperature of 26.3°C, about 2°C above the normal temperature in the surrounding area. Several water wells drilled in the 1950's also indicate that subsurface temperatures in the Lualualei Valley are unusually warm. A shallow hole, drilled deep enough to penetrate the basalt below the alluvium, would provide a more conclusive evaluation of the prospect.

INTRODUCTION

The islands of Hawaii are shield-shaped basaltic domes; therefore, thermal water on these islands owes its heat to volcanic sources. It may well be that the rocks in Hawaii are too permeable to permit steam to accumulate under pressure at levels close to the surface, and the abundance of cold ground water makes unlikely the occurrence of steam at a temperature appreciably above the boiling point (Macdonald and Abbott, 1970). A borehole was drilled at the summit of Kilauea Volcano during the summer of 1973 (Keller, 1974). This study proved that commercial quality steam could be obtained at a practical depth. Undoubtedly, a tremendous amount of volcanic heat exists at relatively shallow depths in the islands of Hawaii.

The Waianae caldera on the island of Oahu is a late Tertiary volcanic center which exhibited resurgent activity during Quaternary period. The study area is located in the Lualualei Valley which is situated to the west of the Waianae Range (see Figs. 1 and 2). Despite the possibility of existence of a heat source, there are no geothermal surface manifestations such as geysers, hot springs, fumaroles, solfatras, etc. Considering the conditions given above, this geophysical investigation was directed to study the area for a buried geothermal system.

A review of geophysical and geologic work done previously by other groups was made. Gravity, magnetic and seismic information helps define the geologic environment of the

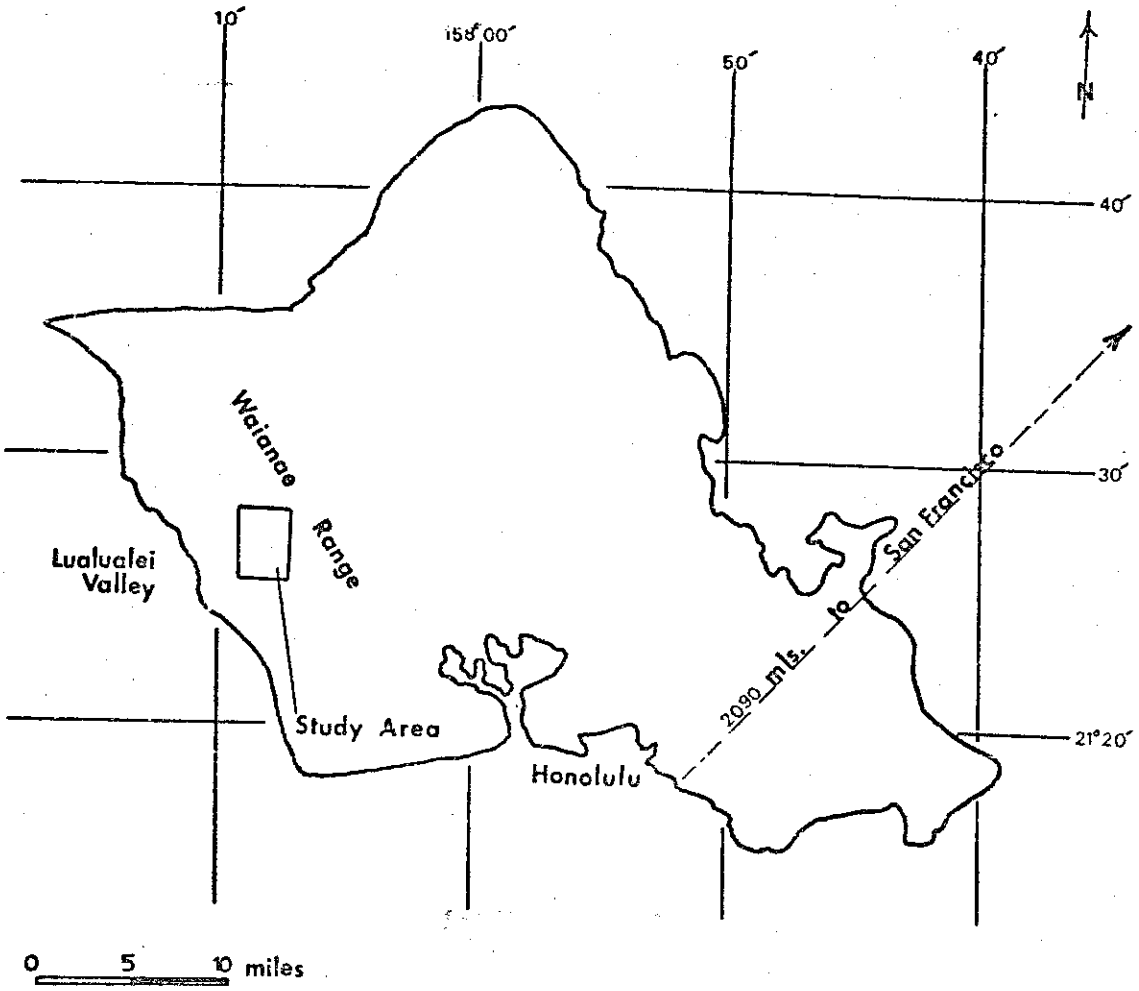

Figure 1. Map of Oahu showing location of the study area.

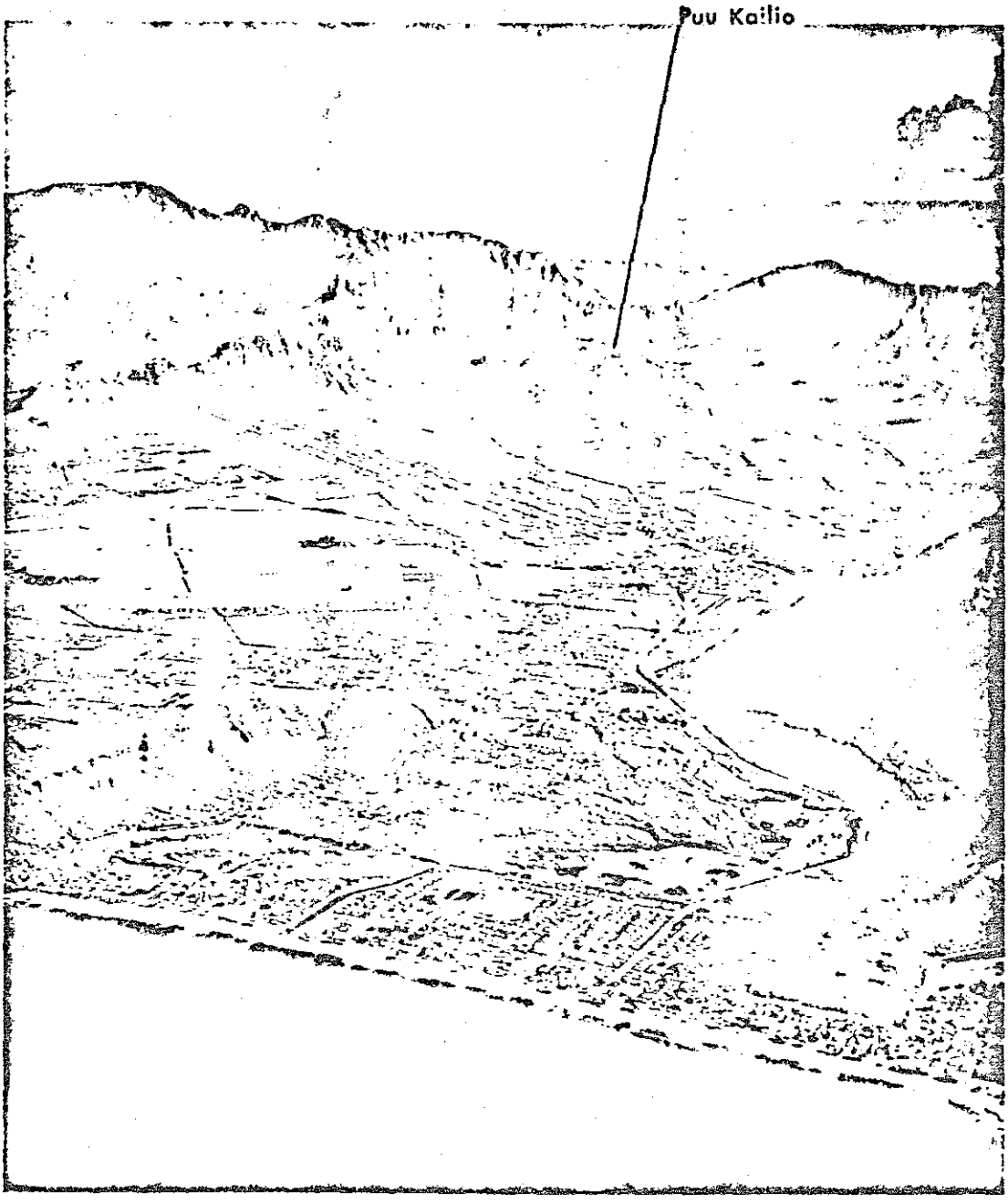

Figure 2. Picture of the Lualualei Valley showing location of the study area (after Macdonald and Abbott, 1970).

study area and its relationship to the volcanic center and the rift zones.

Electrical resistivity methods have been successfully used to locate geothermal reservoirs in different parts of the world for a number of years (Keller, 1970). In order to cover the area in detail and in a short period of time the dipole mapping technique (Furgerson, 1970) was chosen as the main exploration technique. This technique is very effective in mapping lateral resistivity variation and gives a general idea of the vertical variations. Use of one dipole source is not enough to determine best apparent resistivities and anisotropies can cause false anomalies. In order to determine the possibility of observing a false anomaly, two dipole sources at about right angles to each other were set up in the same area. Data from both of these sources were treated together using the rotating-quadripole method to compute the best apparent resistivities. The purpose was to delineate an area with low resistivities, inasmuch as geothermal reservoirs contain water and steam at high temperatures and pressures and dissolved salts; they have higher conductivities than the surrounding rocks.

During the surveys, a relatively conductive zone was discovered. A shallow temperature study was carried out and the results correlated well with the rotating-quadripole data, increasing the likelihood of there being a sealed geothermal reservoir present.

GEOLOGY OF THE AREA

The Hawaiian Islands are a chain of basaltic shield volcanoes built over a fissure 1600 miles long in the ocean floor between 154°40' and 171°75'W longitude and 18°54' to 28"15'N latitude. Recent gravity, magnetic and seismic studies convincingly showed that the lavas which built the Hawaiian islands were extruded primarily along faults oriented either east-west and associated with the Molokai fracture system or northwest-southeast and associated with the trend along which lie the Koolau dike complex and the Musician Seamounts. The volcanic pipes may have formed at points of intersection of rifts of the two fracture systems. Whether the NW-SE fracture system is a strike-slip fault, a simple tension crack or a tear along the crest of a fold is not known. To the southwest of Honolulu at about 1700 feet below sea level, some fossils and shallow-water corals of late Miocene age were discovered (MacDonald and Abbott, 1970). Therefore, the Hawaiian Islands might have been built on an older ridge, perhaps contemporaneous with a chain of islands that existed in middle and early Tertiary time further northwest. The NW-SE fracture system probably has been existent since early Tertiary (Stearns, 1966).

The Hawaiian Islands were built by extrusive materials from volcanic centers during late Tertiary and Quaternary.

The weight of the extruded lavas caused the ridge to sink in order to reestablish isostatic equilibrium. Since the depth to Moho is about 15 km on the Ridge and about 11 km in the normal ocean basin, a thickening of the crust of some 4 km is indicated (Strange, Woollard, and Rose, 1964). Along with volcanism, erosion has taken place. Sea cliffs and drainage systems have been developed. The islands have continued to submerge. The older islands to the northwest are believed to have submerged up to about 9000 feet (Stearns, 1966). Concurrently, a new epoch of volcanism began and secondary outbreaks continued into Recent time. The eruptions occurred on all the major islands except Lanai in Quaternary period. Complex submergences and emergences continued. Because of the rapid alterations of these events very little reef formation took place.

Recently drilled wells in Lualualei Valley penetrated 1200 feet of stream-deposited alluvium before entering lava rock. Since the bottom of the valley is 1200 feet below sea level and the valley had to be cut above sea level, it was concluded that the island must have sunk at least 1200 feet since the alluvium was deposited (MacDonald and Abbott, 1970).

Oahu is a volcanic doublet with an area of 604 square miles and has four major geomorphic provinces. They are: 1) Koolau Range, 2) Waianae Range, 3) Schofield Plateau, and 4) Coastal Plain (see Fig. 3).

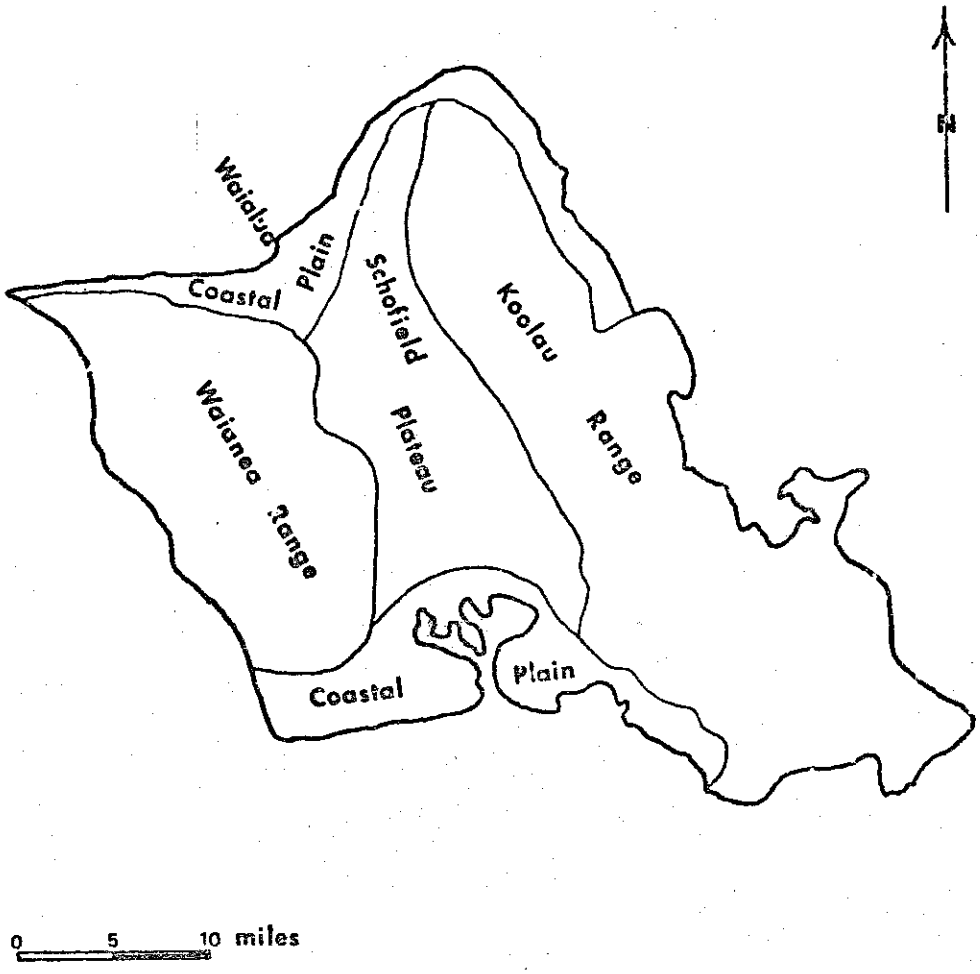

Figure 3. Map of Oahu, showing the major geomorphic provinces (after Stearns, 1966).

The Koolau Range is the younger of the two ranges on the island and it is located to the east. It was built principally by eruptions along a northwest-trending rift zone. The rocks of the Koolau Volcano are mainly tholeiitic basalts and olivine basalts with small amounts of oceanite. They have been divided into two groups. The Kailua Volcanic series are the eroded rocks of the ancient Koolau caldera. These rocks are altered by hydrothermal action due to steam rising in the vent area. The Koolau volcanic series are those lavas and dikes lying outside the caldera and are altered only rarely by hydrothermal action. After the Koolau volcano ceased activity, a period of erosion and deposition started lasting about 2 million years. Then volcanic activity resumed on the southeastern end of the Koolau range. About 30 vents have erupted and they are called the Honolulu volcanic series. The vents are aligned chiefly along NE-SW fissures and the lavas include nephelinites, basanites, and alkalic olivine basalts.

The Waianae Range is located to the west of the island. The Waianae Volcanic series, erupted in Tertiary time, is divided into lower, middle and upper members. The lower member built the main mass of the Waianae shield volcano. It comprises the tholeiitic lava flows and associated pyroclastic rocks. The middle member consists of tholeiitic rocks that accumulated in the caldera, gradually filling it. Alkalic basalts begin to appear toward the top of the middle

member. The upper member is the relatively thin cap that appears to have covered the entire top of the shield late in its history. It is largely hawaiite with lesser amounts of alkalic olivine basalt. See Table 1 for stratigraphic rock units and their ages (Stearns, 1966). Some posterosional eruptions occurred on the Waianae Range, during the Pleistocene, near the ancient caldera. These alkalic olivine basalts are called Kolekole volcanics and they are probably correlative with the secondary eruptions on the Koolau Range.

The Schofield Plateau was formed by the lavas from the Koolau Range banking against the already-eroded slope of the Waianae Volcano to form the gently sloping surface of the Schofield Plateau. An erosional unconformity between the rocks of the two volcanos is visible along Kaukonahua Gulch at the eastern foot of the Waianae Range (MacDonald and Abbott, 1970).

The coastal plain lies mostly on the ponded lavas of the Koolau Volcano north and south of the Schofield Plateau. The plain is composed mainly of marine sediments deposited on the lavas when the sea stood higher in mid-Pleistocene time. See Figure 4 for the geologic map of the island of Oahu.

Geology of the Study Area

After the Waianae Volcano ceased activity, stream erosion began and great valleys were carved, especially on the southwest side of the Waianae Range where the streams were older and the rocks weaker. Then the island went through a complex cycle of submergences and emergences (Stearns, 1966). The

Table 1. Stratigraphic rock units in the island of Oahu (after Stearns, 1966).

Age	Waianae Range	Koolau Range
Historic	Coral fill	Coral fill
Recent	Younger alluvium and consolidated calcareous beach and dune deposits	Younger alluvium, unconsolidated beach and dune deposits, and younger rocks in the Honolulu volcanic series
	Local Unconformity	
Pleistocene	Lithified calcareous dunes, emerged marine limestone, older alluvium, and Kolekole volcanics	Lithified calcareous dunes, emerged marine limestone, older alluvium, and older rocks in the Honolulu volcanic series
	Great Erosional Unconformity	
Pliocene and Older	Waianae volcanic series; upper, lower and middle members	Koolau and Kailua volcanic series

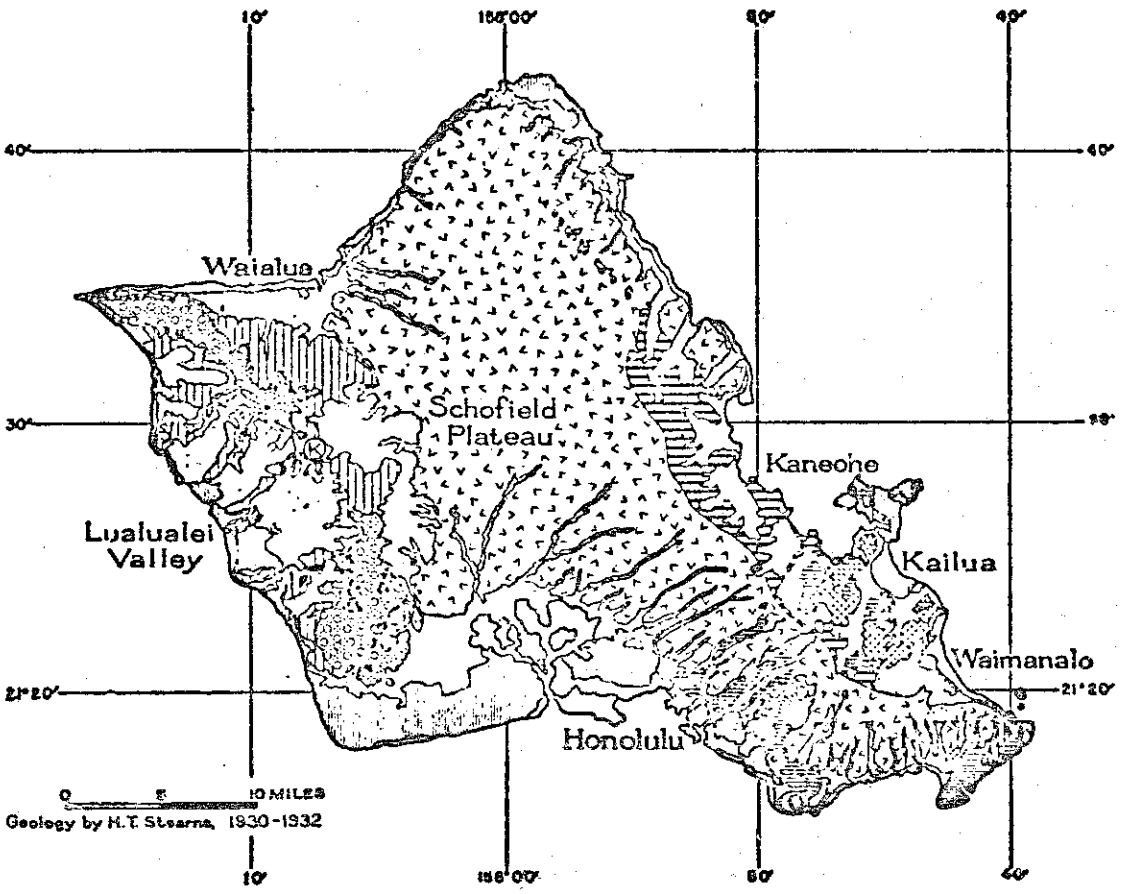

SEDIMENTARY ROCKS

RECENT — PLEISTOCENE

Beach and dune sand | Alluvium | Limestone (Reefs and dunes)

VOLCANIC ROCKS

KOOLAU RANGE — WAIANAE RANGE

QUATERNARY

Lavas — Pyroclastics — Honolulu volcanic series

Kolekole volcanics

EROSIONAL UNCONFORMITY

TERTIARY

Flows — Dike complex

Caldera complex: Lava flows; Vent breccia; Dike complex — Koolau volcanic series

Upper member: Cone; Vent breccia

Lower and middle members — Waianae volcanic series

Figure 4. Geologic map of the island of Oahu (after Stearns, 1946)

great submergence resulted in deep drowning of the great valleys and their subsequent sedimentation. Re-emergence of Oahu exposed the great valleys to erosion once more, with their nearly flat alluvial plains. The area is located at the northeast corner of one of these valleys, namely the Lualualei Valley.

The study area is covered with alluvium. The exact thickness of alluvium in the vicinity of the anomaly is not known; however, it is believed to be about 1200 feet (probably less than 1200 feet), since drill holes penetrated 1000 feet of alluvium near the town of Waianae and 1200 feet in the Lualualei Valley (MacDonald and Abbott, 1970). It is expected to get thinner towards the steep walls of the valley, to the east, the north and the south. Outcrops in the eastern and the northeastern part of the area are believed to be from the Lower Member of the Waianae Volcanic Series. Kolekole volcanics which was the result of renewed volcanism in the Pleistocene time is located three miles to the northeast of the anomaly (Fig. 4). The caldera of the Waianae Volcano was located in the area immediately west of Kolekole Pass, and extended from the northern side of Makaha Valley to the head of Nanakuli Valley (Fig. 5). This puts the study area close to the center of the caldera. Near the area where the Lower and the Middle members of the Waianae Volcanic Series are exposed, there are numerous dikes. Their sizes vary between a few inches and 15 feet, and most of them are nearly vertical with a general trend parallel to the rift zones.

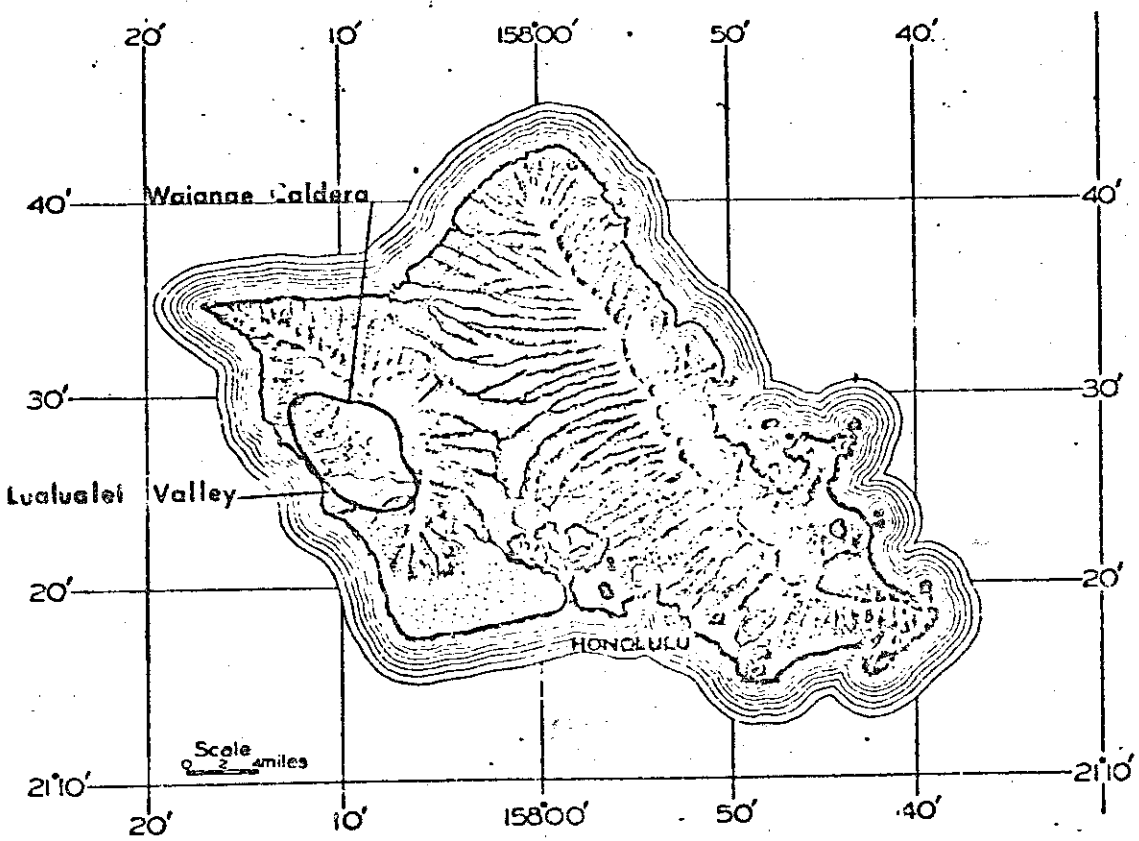

Figure 5. Shaded relief map of the island of Oahu, showing location of the Waianae Caldera (after Stearns, ~~1939~~ 1966)

There are no faults large enough to justify individual descriptions in or near the study area. Numerous dikes of different sizes suggests lateral displacement and jointing of the host rock with each injection. Puu Kailio, which is a hill located at the head of Lualualei Valley, was a place of intense volcanic activity; therefore, it was decided that the Kailio syncline was merely a sag in the flows produced by local withdrawal of support (Stearns, 1966). The anomaly is located about 2.5 miles south-southwest of this syncline (Fig. 2).

SURVEY TECHNIQUES

Rotating-Quadripole Survey

Description of the Method: The rotating-quadripole technique is an electrical resistivity method which makes use of two dipole sources oriented at approximately right angles to each other. In fact, conventional dipole mapping procedures were used in the field (Furgerson, 1970, and Jordan, 1974); however, the data were treated differently.

A suitable location was selected to set up a fixed d-c current source, keeping in mind the boundaries of the study area. Then, two holes 800 meters apart, were dug to bury two tin sheets, 3 feet by 4 feet. In order to reduce the contact resistance, salt and water were used. These two source electrodes were connected with #12 insulated, copper wire. To generate an electric field, a 2.5 kw generator was used. The 1-phase, 120v a-c, 60 hz output of the generator was passed through an asymmetrically-timed switching circuit and then rectified to d-c current. The asymmetric square-wave output of the rectifier was fed into the source wire. The relative polarity of the voltage drop along receiver wire was determined by observing the asymmetry of the square-wave output.

The field measurements were made a quarter of a mile apart from each other along the roads and near the ammunition magazines. At every station, two components (preferably orthogonal) of the earth potential were measured. To do this, two non-polarizing receiver electrodes were placed 30 meters

apart and connected to a d-c amplifier with #12 insulated copper wire. The output of the amplifier was recorded with a potentiometric chart recorder. A Brunton Compass was used to determine azimuths of both components. Measurements were made at 103 stations around the first source. Then the second source was set up at a 96° angle to the first source. Measurements were repeated occupying the same stations.

Two voltage components for each source were divided by the receiver length (30 m) to obtain electric field components and added vectorially to determine the total electric fields for both sources. If both sources were turned on, there would be only one total electric field and it can be obtained by orthogonal addition of the total electric fields of the two sources. The fields from the two sources can also be added with appropriate weights to rotate the total electric field 180°. A set of apparent resistivities for every station was calculated using the rotating quadripole equation (see Appendix A-1 for the equation, and Appendix A-2 for the data obtained in the field). Out of 40 resistivity values the best (the highest) value was selected for every station.

Interpretation of Field Data

Best Apparent Resistivity: The dipole mapping technique has been used extensively to determine lateral resistivity variations due to conductive bodies at depth, such as geothermal reservoirs. This fast d-c resistivity method also reveals information about the geologic structure of an area

provided a resistive basement is present, and can be used for depth estimates. However, the technique is not problem free. Presence of a fault-like boundary between the region with moderate resistivities and another region with high resistivities will cause "false" anomalies to be observed at specific locations along the fault-like boundary (Fig. 6) (Grose and Keller, 1974).

To eliminate the observed false anomalies and to obtain resistivities as close as possible to the true resistivities multiple coverage must be provided. This can be done by randomly located multiple sources or by the rotating-quadripole method. In the rotating quadripole method, two dipole sources at right angles to each other are used.

Out of 40 resistivity values obtained by rotating the total electric field, the highest value was picked for every station. These values are believed to be the closest to the true resistivities; therefore, they were called the best apparent resistivities. In almost all cases the best resistivities are higher than the resistivities obtained from the original dipole source.

Figure 7 shows the best apparent resistivity map of the study area. The 75 ohm-m contours and high resistivities indicate the presence of a resistive basement at depth. The resistive basement is believed to be the volcanic plug of the Waianae Volcano. A closed 35 ohm-m contour near the sources indicates the presence of a thin conductive surface layer.

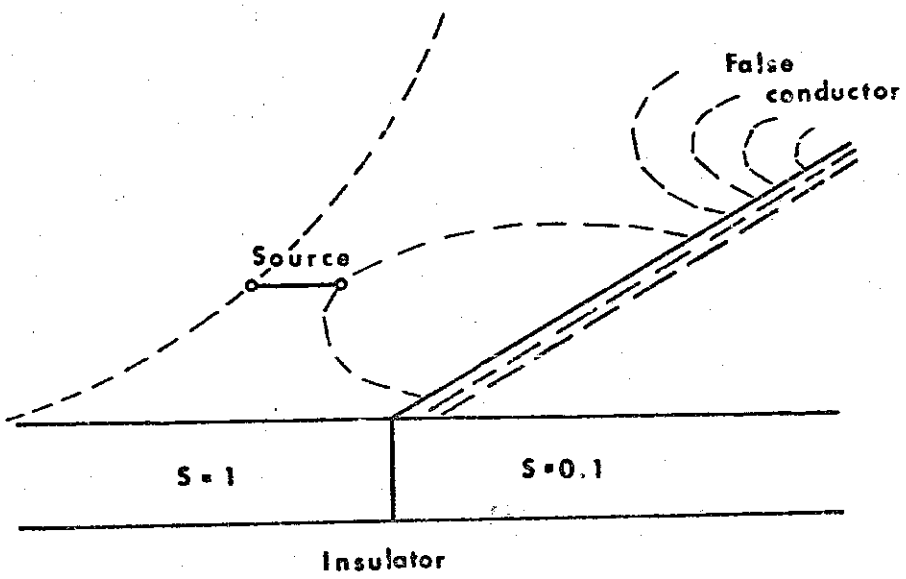

Figure 6. Observed false conductor along the fault like boundary (after Grose and Keller, 1974)

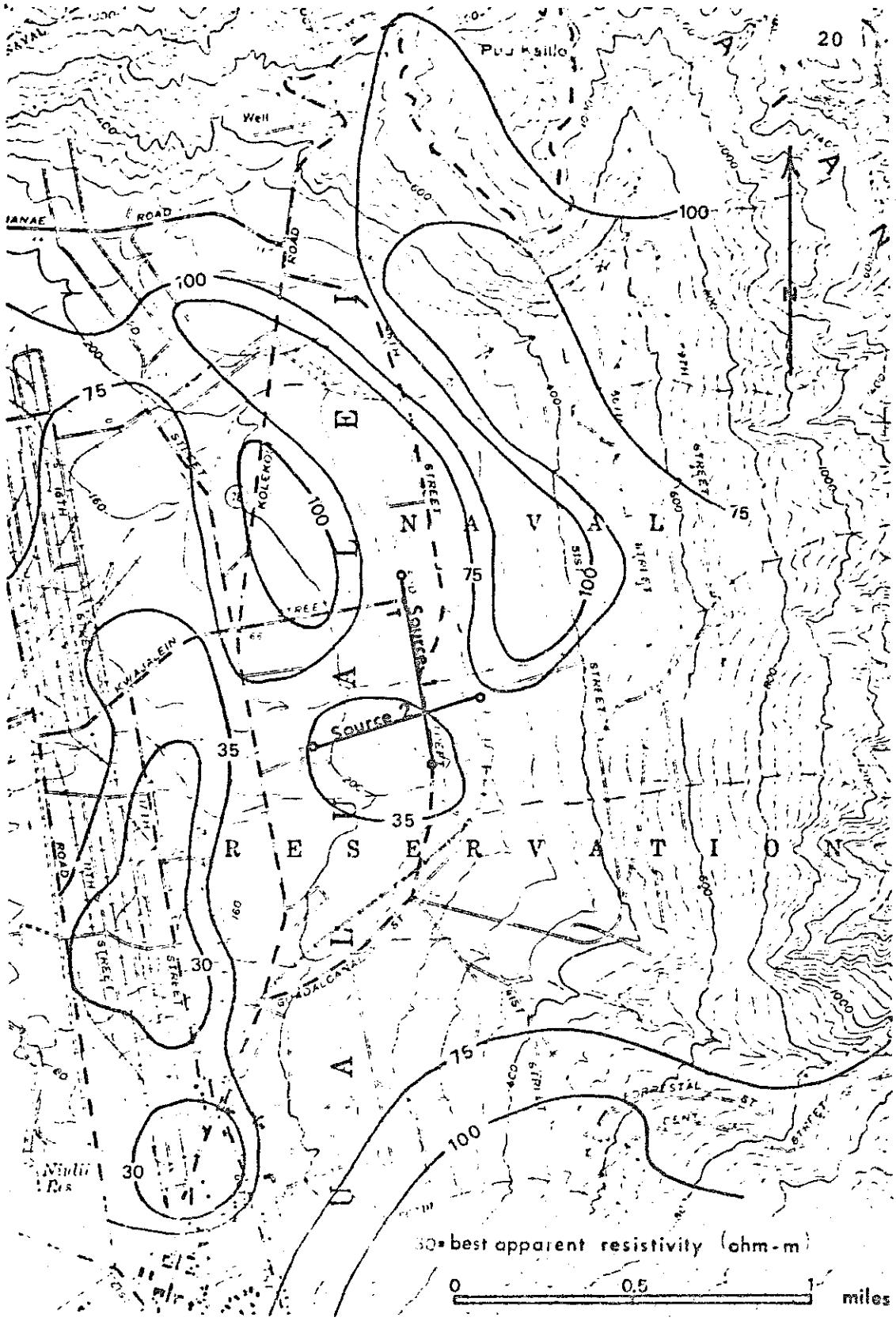

Figure 7. Best apparent resistivity map of the Lualualei Naval Magazine -- rotating-quadripole array

The 35 and 30 ohm-m contours to the southwest of the sources might be caused by a conductive body at depth.

A histogram showing the distribution of best resistivity values is presented in Fig. 8. A deviation from a normal distribution occurs between 28 and 41.4 ohm-m, and these anomalous values were measured mainly in the conductive zone located to the southwest of the two sources (Magazines 11 and 12).

To construct a scatter diagram, best resistivities were plotted against the distance to the nearest of the four source electrodes. This distance is thought to be the depth of current penetration. The resulting scatter diagram (Fig. 9) suggests the presence of layering in the area, because the points tend to cluster along a 45° angle after 1 km distance.

Temperature Survey

Geothermal exploration should not be limited to the vicinity of areas of heat escape in the form of geysers, fumaroles, sulfatras and hot springs. A reservoir of moderate size with an upper surface at 2 km depth would approximately double the normal geothermal gradient over an area of a few square kilometers (Banwell, 1970). Therefore, detection of a sealed reservoir with no convection to the surface is not difficult. Surface temperature and heat flow measurements at 1 to 2 m depths have been successful in mapping high temperature zones and in evaluating the hot water distribution below the surface. Such observations provide a rapid and direct way of making an estimate of the size and

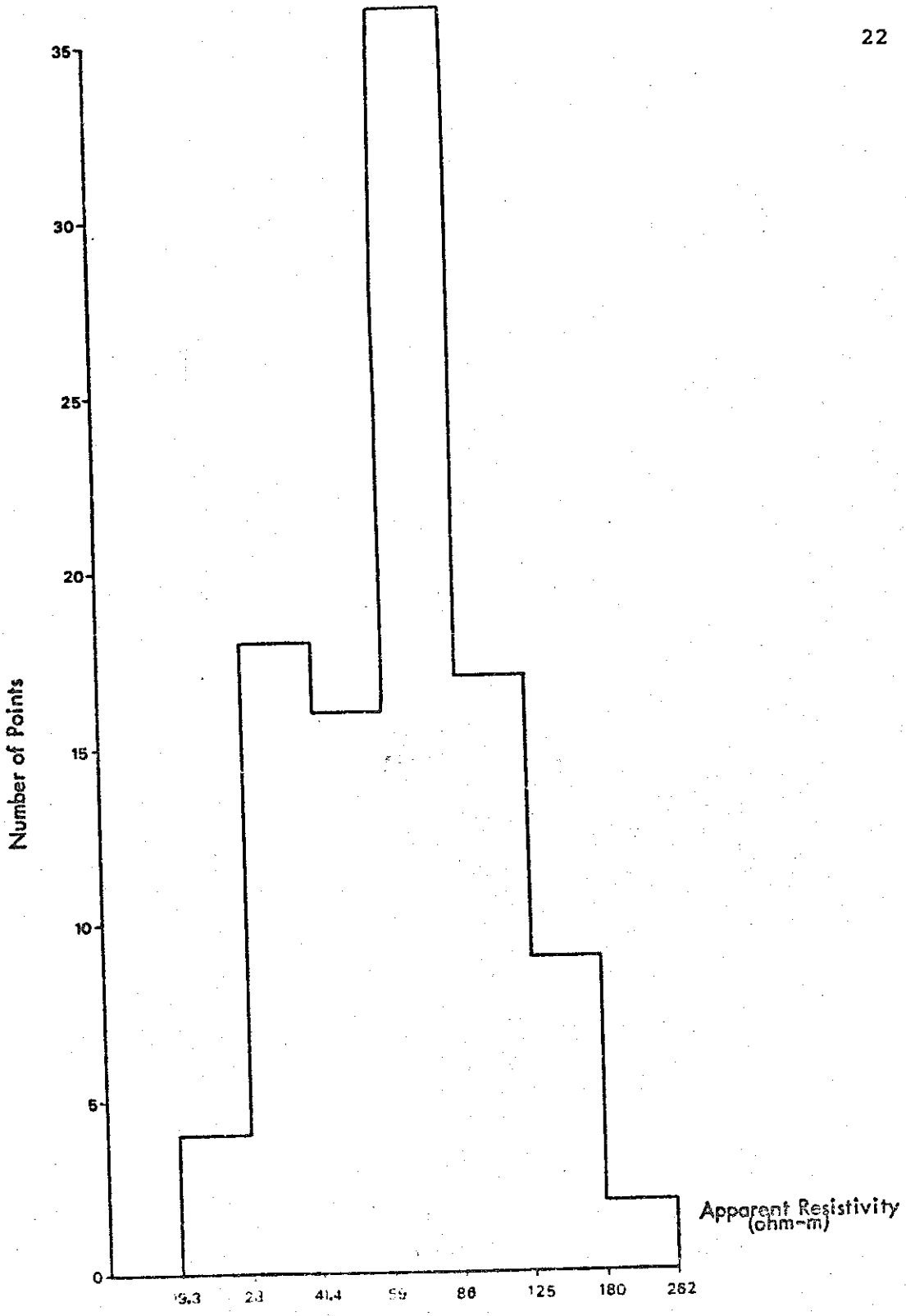

Figure 8. Distribution of best apparent resistivity -- rotating-quadripole (rrc/

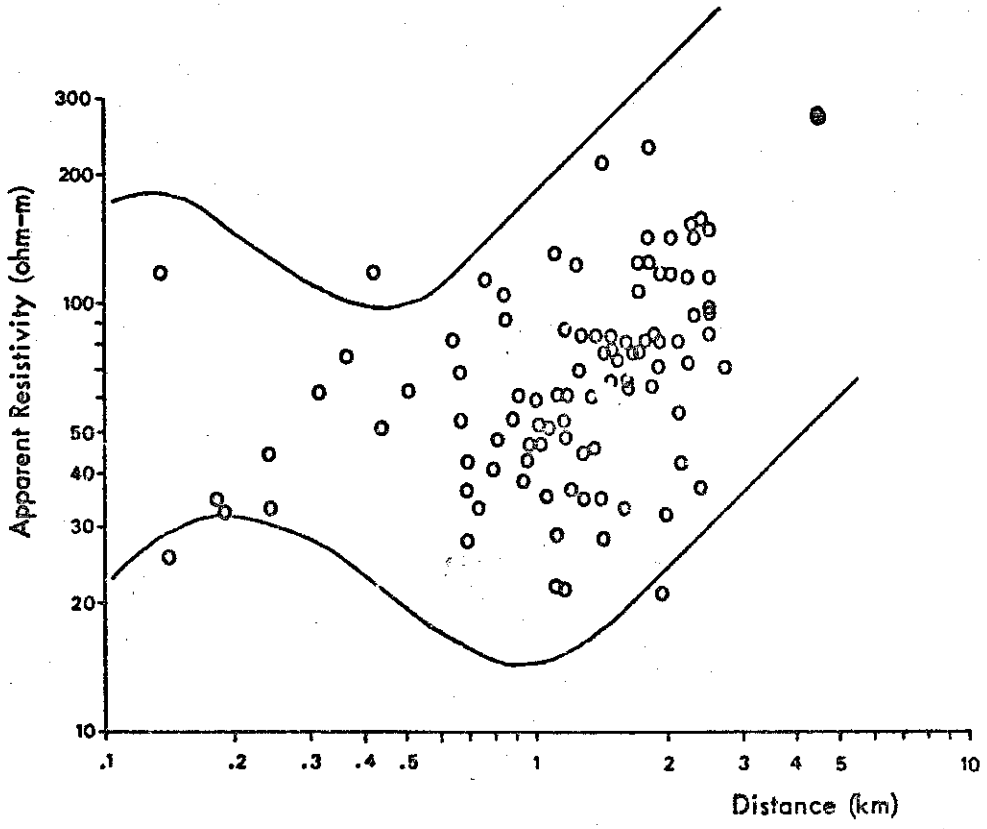

Figure 9. Best apparent resistivity scatter diagram -- rotating-quadripole array

energy potential of a system. When making or interpreting a shallow temperature survey, hydrological conditions in the area including rate and direction of ground water movement have to be considered. Because movement of ground water can carry away the conductive heat flow from a thermal anomaly, it can displace the surface temperature patterns. Instrumental errors may result from using thermistor probes for temperature measurements; the overall error has been estimated to be between 0.01 and 0.05°C for measurements at a depth of 2 m (Dedkova, et al, 1970). Seasonal and weather changes and variations in surface cover are believed to have random effects on shallow temperatures.

Description of the Method: A shallow (1 meter deep) temperature study was carried out in the Lualualei Naval Magazine in order to determine the shallow temperature distribution and locate areas with anomalous temperature gradients. A simple mechanical device called a dongeyknocker made of mild steel was used to punch holes in the ground. A precision thermistor teflon probe was placed at the bottoms of these holes using a wooden rod. The resistance of the probe was measured with a digital multimeter. These resistances were converted to temperatures (°C) using a conversion table. The measurements were spaced closely (800 feet apart) over the resistivity anomaly to provide detail in that area. A wider spacing of 2000 feet was used for the measurements over the resistive zone. A total of 70 measure-

ments was made including 7 to the west of the Fence Road where there is no resistivity information.

Interpretation of the Field Data

Ground Temperature: Measured temperature values represent ground temperatures and Fig. 10 shows the ground temperature (at 1 meter depth) pattern of the area. Before making an attempt to interpret the data, some important factors should be considered. Surface cover in the area is alluvium and major variations likely to cause false anomalies are unlikely. Since there is a difference of 2°C in temperatures between the cold and the warm zones, instrumental errors (.05°C or less) could not have changed the temperatures enough to distort the temperature pattern. Where ground water is confined between dikes, it is under static conditions. This is true for the basalts with numerous dikes below the alluvial fill; however, the alluvial section itself is believed to contain water under dynamic conditions.

It was discovered that the area with anomalous resistivities (less than 30 ohm-m) had, in general, a temperature of 26.3°C. Since the resistive zones had lower ground temperatures (as low as 24.3°C), it was concluded that the low resistivities to the southwest of the dipoles were caused by high temperatures at depth, possibly a sealed geothermal reservoir. The other temperature anomalies in the area (areas with temperatures higher than 26°C) are believed to be surficial features caused either by variations in the

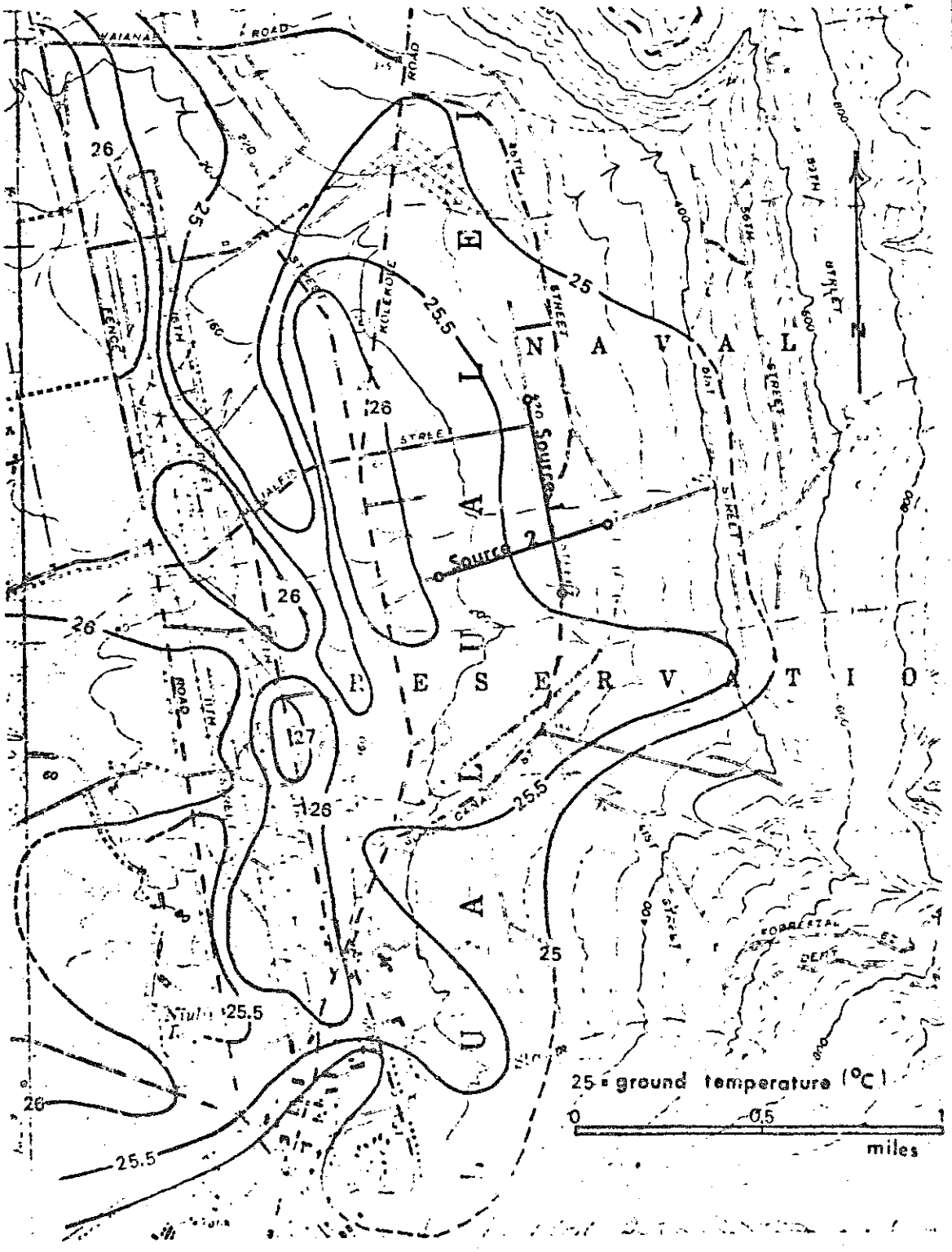

Figure 10. Ground temperature map of the Lualualei Naval Magazine, based on measurements made at 1 m depth

surface cover or by the movement of the ground water in alluvium or both, and they are not supported by low resistivities except where there is no resistivity information.

Self-Potential Survey

Geothermal reservoirs contain ground water of differing temperature and chemical composition. Thermal gradients in pore water electrolytes and contact potentials between bodies of ground water of differing temperature and chemical composition may give rise to measurable electrical anomalies. In the course of resistivity surveys of thermal areas, high natural electrical potentials have been commonly observed (Banwell, 1970). These natural potentials may form a diagnostic pattern over the area. Such a survey would be valuable since it would have some depth penetration and point by point observations would be possible with small electrode spacings.

Description of the Method: A self-potential survey was carried out in order to determine if the area with low resistivities and high temperatures had anomalous self potentials. The measurements were made with a digital voltmeter using two non-polarizing electrodes with an electrode spacing of 200 m. A starting point with an assigned potential of zero was picked in an area with high resistivities (Fig. 11). Potential drops were measured along a continuous line, across

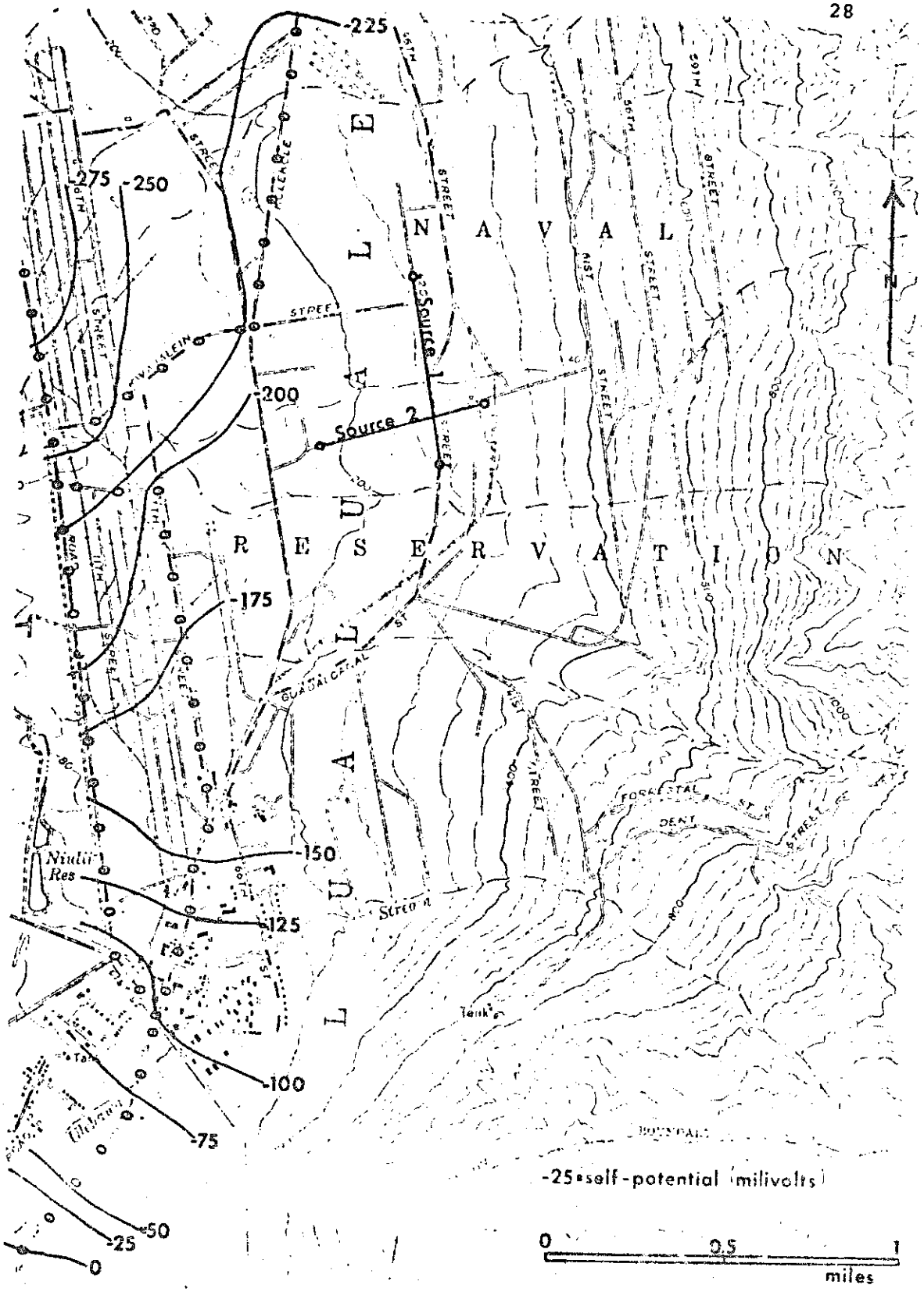

Figure 11. Self-potential map of the Lualualei Naval Magazine

the area of interest, ending in an area with high resistivities. A loop was made around the anomaly to distribute the total error among individual measurements.

Interpretation of Field Data

Self Potential: After error distribution (2 mv/200 m), potential drops with respect to the initial point with zero potential were calculated. Contoured self-potential values are shown in Fig. 11. Self-potential over the area decreases, in general, to the north and there is no indication of an anomalous pattern in the area with low resistivities and high temperatures.

CONCLUSIONS AND RECOMMENDATIONS

Does the area where the Lualualei Naval Magazine is located have a geothermal reservoir? If so, does it contain high enthalpy water at an economical depth? These were the questions under consideration during the course of this study.

The area is located near a center of intense volcanism (Puu Kailio) inside the volcanic vent zone of the Waianae Caldera. Even though the Waianae Range was built in late Tertiary, the volcanism continued during the Quaternary period. Young volcanism in the area suggests the presence of a strong and active heat source. All geophysical work done in the area indicates the presence of a dense body of rock extending from shallow depths (800 m from the surface) to a depth of 5.5 km under the Waianae Caldera. It is probable that olivine and perhaps other heavy crystals that have lagged behind in basaltic magma rising toward the surface, and have accumulated to form a plug of peridotite that resembles mantle rock in its physical properties. The drill hole at the summit of Kilauea penetrated rocks with low permeability and densities around 3.2 gr/cc. The volcanic plug under the Waianae Caldera is believed to be made up of rocks similar to the rocks found under the Kilauea Volcano. Low permeability probably minimized the heat escape from the heat source; thus, maintaining its heat content over the years. The geological conditions in the area indicate the presence of a heat source.

The rocks located above the volcanic plug are believed to be highly fractured due to a high number of dikes of different sizes. Since these highly permeable basalts are located above the possible heat source, and since the area has abundant groundwater due to high rainfall, the section between the volcanic plug and the alluvial fill has the properties to behave as the reservoir rock for a geothermal system. The area where the anomaly is located may have up to 1000 feet of alluvium on the surface. The alluvium (Pleistocene) is believed to be partially consolidated and inasmuch as it is located above the permeable basalts, and there is a possibility of hydrothermal alteration, the alluvium could behave like a caprock because of its reduced permeability. Presence of a zone with low permeability over the reservoir minimizes the heat escape to the surface, keeping most of the heat in the reservoir, thus increasing the temperature of the groundwater. From the discussion above, it can be concluded that the geologic environment is suitable for presence of a geothermal system.

To locate the area with anomalous geothermal gradient, a rotating-quadripole survey was carried out. Anomalous low resistivities were discovered to the southwest of the dipole sources. A shallow temperature study which was done afterwards confirmed that the low resistivities were caused by high temperatures in the area. Because there is no surface activity, chemical analyses to determine the reservoir temperature were not available. Temperature measurements made

at a meter depth could not be used to determine the true geothermal gradient.

As a result of this study, it is concluded that the area where magazines 11 and 12 are located may have a sealed geothermal reservoir at depth. However, the vertical resistivity distribution and the temperature gradient in the area are not known. A test hole which is deep enough to penetrate the basalts below the alluvium should be drilled to determine the temperature gradient and also to obtain valuable information about the rocks in the area. Perhaps a number of initial test holes with intermediate depths (20 m) could be drilled to determine the hottest part of the anomalous area.

APPENDIX A-1

DERIVATION OF APPARENT RESISTIVITY EXPRESSION FOR THE ROTATING-QUADRIPOLE ARRAY

Take two dipole sources at approximately right angles to each other. Even though it is desirable, they do not have to have a common electrode.

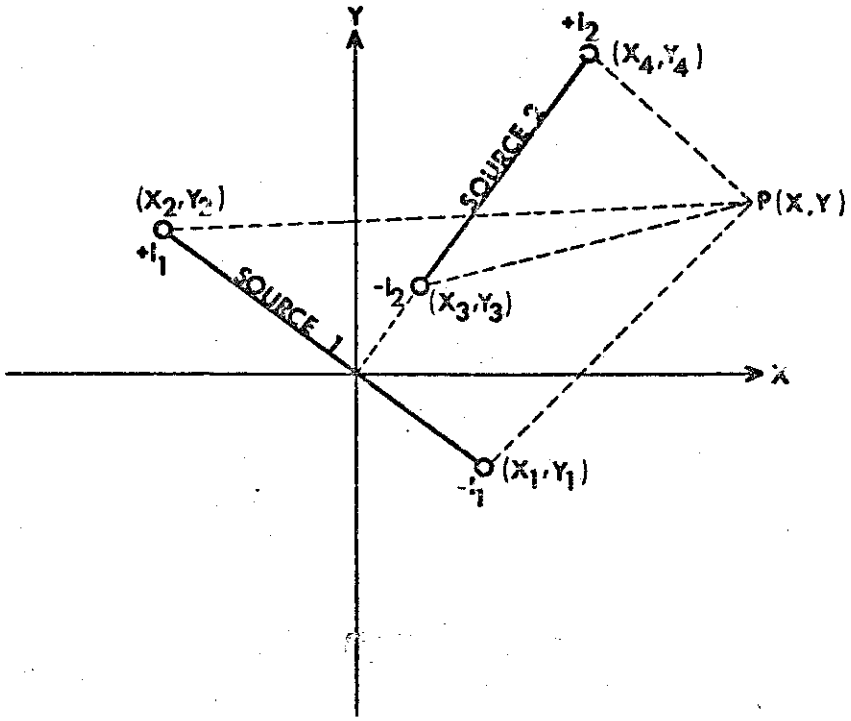

The potential expression for apparent resistivity assuming spherical current spreading from single electrode in a homogeneous earth is $u = \rho I/2\pi R$ (Van Nostrand and Cook, 1966). The potential at point P due to all four electrodes can be written.

$$U_1 = -\rho I_1/2\pi[(x-x_1)^2+(y-y_1)^2]^{1/2}$$

$$U_2 = +\rho I_1/2\pi[(x-x_2)^2+(y-y_2)^2]^{1/2}$$

$$U_3 = -\rho I_2/2\pi[(x-x_3)^2+(y-y_3)^2]^{1/2}$$

$$U_4 = +\rho I_2/2\pi[(x-x_4)^2+(y-y_4)^2]^{1/2}$$

Since $\vec{E} = -\vec{\nabla}U$, $E_x = -\partial U/\partial x$ and $E_y = -\partial U/\partial y$

x and y components of the electric field at point P due to all four electrodes:

$$E_{1x} = \rho I_1(x-x_1)/2\pi[(x-x_1)^2+(y-y_1)^2]^{3/2}$$

$$E_{1y} = \rho I_1(y-y_1)/2\pi[(x-x_1)^2+(y-y_1)^2]^{3/2}$$

$$E_{2x} = -\rho I_1(x-x_2)/2\pi[(x-x_2)^2+(y-y_2)^2]^{3/2}$$

$$E_{2y} = -\rho I_1(y-y_2)/2\pi[(x-x_2)^2+(y-y_2)^2]^{3/2}$$

$$E_{3x} = \rho I_2(x-x_3)/2\pi[(x-x_3)^2+(y-y_3)^2]^{3/2}$$

$$E_{3y} = \rho I_2(y-y_3)/2\pi[(x-x_3)^2+(y-y_3)^2]^{3/2}$$

$$E_{4x} = -\rho I_2(x-x_4)/2\pi[(x-x_4)^2+(y-y_4)^2]^{3/2}$$

$$E_{4y} = -\rho I_2(y-y_4)/2\pi[(x-x_4)^2+(y-y_4)^2]^{3/2}$$

The total electric fields in x and y directions are:

$$E_{Tx} = \frac{\rho}{2\pi}\left\{\frac{I_1\,(x-x_1)}{[(x-x_1)^2+(y-y_1)^2]^{3/2}} - \frac{I_1\,(x-x_2)}{[(x-x_2)^2+(y-y_2)^2]^{3/2}}\right.$$

$$\left. + \frac{I_2\,(x-x_3)}{[(x-x_3)^2+(y-y_3)^2]^{3/2}} - \frac{I_2(x-x_4)}{[(x-x_4)^2+(y-y_4)^2]^{3/2}}\right\}$$

$$E_{Ty} = \frac{\rho}{2\pi}\left\{\frac{I_1\,(y-y_1)}{[(x-x_1)^2+(y-y_1)^2]^{3/2}} - \frac{I_1\,(x-x_2)}{[(x-x_2)^2+(y-y_2)^2]^{3/2}}\right.$$

$$\left. + \frac{I_2\,(y-y_3)}{[(x-x_3)^2+(y-y_3)^2]^{3/2}} - \frac{I_2\,(y-y_4)}{[(x-x_4)^2+(y-y_4)^2]^{3/2}}\right\}$$

The amplitude of the total electric field at point P is:

$$E_{TOT} = (E_{Tx}^2 + E_{Ty}^2)^{1/2}$$

Let:

$$R_1 = [(x-x_1)^2 + (y-y_1)^2]^{1/2}$$

$$R_2 = [(x-x_2)^2 + (y-y_2)^2]^{1/2}$$

$$R_3 = [(x-x_3)^2 + (y-y_3)^2]^{1/2}$$

$$R_4 = [(x-x_4)^2 + (y-y_4)^2]^{1/2}$$

Substitute four equations above in the equation for E_{TOT}

$$E_{TOT} = \frac{\rho}{2\pi}\left\{\left[\frac{I_1(x-x_1)}{R_1^3} - \frac{I_1(x-x_2)}{R_2^3} + \frac{I_2(x-x_3)}{R_3^3} - \frac{I_2(x-x_4)}{R_4^3}\right]^2\right.$$

$$\left. + \left[\frac{I_1(y-y_1)}{R_1^3} - \frac{I_1(x-x_2)}{R_2^3} + \frac{I_2(y-y_3)}{R_3^3} - \frac{I_2(y-y_4)}{R_4^3}\right]^2\right\}^{1/2}$$

$$E_{TOT} = \frac{\rho}{2\pi}\left\{\frac{I_1^2(x-x_1)^2}{R_1^6} + \frac{I_1^2(x-x_2)^2}{R_2^6} + \frac{I_2(x-x_3)^2}{R_3^6} + \frac{I_2(x-x_4)^2}{R_4^6}\right.$$

$$- \frac{2I_1^2(x-x_1)(x-x_2)}{R_1^3R_2^3} + \frac{2I_1I_2(x-x_1)(x-x_3)}{R_1^3R_3^3}$$

$$- \frac{-2I_1I_2(x-x_1)(x-x_4)}{R_1^3R_4^3} - \frac{-2I_1I_2(x-x_2)(x-x_3)}{R_2^3R_3^3}$$

$$+ \frac{2I_1I_2(x-x_2)(x-x_4)}{R_2^3R_4^3} - \frac{2I_2^2(x-x_3)(x-x_4)}{R_3^3R_4^3}$$

$$+ \frac{I_1^2(y-y_1)^2}{R_1^6} + \frac{I_1^2(y-y_2)^2}{R_2^6} + \frac{I_2^2(y-y_3)^2}{R_3^6}$$

$$+ \frac{I_2^2(y-y_4)}{R_4^6} - \frac{2I_1^2(y-y_1)(y-y_2)}{R_1^3R_2^3}$$

$$+ \frac{2I_1I_2(y-y_1)(y-y_3)}{R_1^3R_3^3} - \frac{2I_1I_2(y-y_1)(y-y_4)}{R_1^3R_4^3}$$

$$- \frac{2I_1I_2(y-y_2)(y-y_3)}{R_2^3R_3^3} + \frac{2I_1I_2(y-y_2)(y-y_4)}{R_2^3R_4^3}$$

$$\left. - \frac{2I_2^2(y-y_3)(y-y_4)}{R_3^3R_4^3}\right\}^{1/2}$$

$$E_{TOT} = \frac{\rho}{2\pi}\left\{\frac{I_1^2}{R_1^6}\left[(x-x_1)^2+(y-y_1)^2\right] + \frac{I_1^2}{R_2^6}\left[(x-x_2)^2+(y-y_2)^2\right]\right.$$

$$+ \frac{I_2^2}{R_3^6}\left[(x-x_3)^2+(y-y_3)^2\right] + \frac{I_2}{R_4^6}\left[(x-x_4)^2+(y-y_4)^2\right]$$

$$- \frac{2I_1^2}{R_1^3R_2^3}\left[(x-x_1)(x-x_2) + (y-y_1)(y-y_2)\right]$$

$$- \frac{2I_1I_2}{R_1^3R_3^3}\left[(x-x_1)(x-x_3) + (y-y_1)(y-y_3)\right]$$

$$- \frac{2I_1I_2}{R_1^3R_4^3}\left[(x-x_1)(x-x_4) + (y-y_1)(y-y_4)\right]$$

$$- \frac{2I_1I_2}{R_2^3R_3^3}\left[(x-x_2)(x-x_3) + (y-y_2)(y-y_3)\right]$$

$$+ \frac{2I_1I_2}{R_2^3R_4^3}\left[(x-x_2)(x-x_4) + (y-y_2)(y-y_4)\right]$$

$$\left. - \frac{2I_2}{R_3^3R_4^3}\left[(x-x_3)(x-x_4) + (y-y_3)(y-y_4)\right]\right\}^{1/2}$$

Let: $C = I_1/I_2$ and substitute this equation in the last equation for E_{TOT} above.

$$E_{TOT} = \frac{\rho I_2}{2\pi}\left(\frac{C^2}{R_1^4} + \frac{C^2}{R_2^4} + \frac{1}{R_3^4} + \frac{1}{R_4^4}\right.$$

$$- \frac{2C^2}{R_1^3 R_2^3}\left[(x-x_1)(x-x_2) + (y-y_1)(y-y_2)\right]$$

$$+ \frac{2C}{R_1^3 R_3^3}\left[(x-x_1)(x-x_3) + (y-y_1)(y-y_3)\right]$$

$$- \frac{2C}{R_1^3 R_4^3}\left[(x-x_1)(x-x_4) + (y-y_1)(y-y_4)\right]$$

$$- \frac{2C}{R_2^3 R_3^3}\left[(x-x_2)(x-x_3) + (y-y_2)(y-y_3)\right]$$

$$+ \frac{2C}{R_2^3 R_4^3}\left[(x-x_2)(x-x_4) + (y-y_2)(y-y_4)\right]$$

$$\left. - \frac{2}{R_3^3 R_4^3}\left[(x-x_3)(x-x_4) + (y-y_3)(y-y_4)\right]\right)^{1/2}$$

Call that part of the equation in parentheses K.

$$E_{TOT} = \frac{\rho I_2}{2\pi} K, \quad \rho = \frac{2\pi E_{TOT}}{I_2 K}$$

The expression for apparent resistivity is

$$\rho = \frac{2\pi E_{TOT}}{I_2 K}$$

where K is the geometric factor. To find the apparent resistivity expressions for dipoles one and two individually, let $I_2 = 0$ and $I_1 = 0$ respectively in the composite equation for the rotating-quadripole array above.

Let:

$$I_2 = 0$$

$$E_{TOT_1} = \frac{\rho I_1}{2\pi}\left\{\frac{1}{R_1^4} + \frac{1}{R_2^4} - \frac{2}{R_1^3 R_2^3}\left[(x-x_1)(x-x_2)+(y-y_1)(y-y_2)\right]\right\}^{1/2}$$

$$E_{TOT_1} = \frac{\rho I_1}{2\pi} K_1$$

$$\rho = \frac{2\pi E_{TOT_1}}{I_1 K_1}$$: Apparent resistivity equation for the first source.

Let:

$$I_1 = 0$$

$$E_{TOT_2} = \frac{\rho I_2}{2\pi}\left\{\frac{1}{R_3^4} + \frac{1}{R_4^4} - \frac{2}{R_3^3 R_4^3}\left[(x-x_3)(x-x_4)+(y-y_3)(y-y_4)\right]\right\}^{1/2}$$

$$E_{TOT_2} = \frac{\rho I_2}{2\pi} K_2$$

$$\rho = \frac{2\pi E_{TOT_2}}{I_2 K_2}$$: Apparent resistivity equation for the second source.

APPENDIX A-2

ROTATING-QUADRIPOLE MAPPING FIELD DATA

N : Station number

R : Distance from measuring point to the origin (the intersection point of the two sources)(km)

REAR: Azimuth of the line between the origin and the receiver station (degrees)

B1 : Azimuth of the first receiver line (source #1)(degrees)

B2 : Azimuth of second receiver line (source #1)(degrees)

BR1 : Azimuth of first receiver line (source #2)(degrees)

BR2 : Azimuth of second receiver line (source #2)(degrees)

EX1 : Voltage measured along first receiver line (source #1)(mv)

EY1 : Voltage measured along second receiver line (source #1)(mv)

EX2 : Voltage measured along first receiver line (source #2) (mv)

EY2 : Voltage measured along second receiver line (source #2)(mv)

CUR1: Total step current on source #1 (amperes)

CUR2: Total step current on source #2 (amperes)

XL : Length of receiver line (meters)

R1 : Resistivity due to source #1 (ohm-m)

R2 : Resistivity due to source #2 (ohm-m)

Rmax: Maximum resistivity (ohm-meters)

Rmin: Minimum resistivity (ohm-meters)

RTO : Ratio of maximum to minimum resistivity

N	R	BEAR	B1	B2	BR1	BR2	EX1	EY1	EX2	EY2	CUR1	CUR2	XL	R1	R2	R_{max}	R_{min}	RTO
1	0.021	112	186	287	180	256	-18500	5000	-6500	-12500	4.5	3.5	30	26.5	34.3	35.0	26.4	1.3
2	1.067	351	174	76	175	75	3200	-140	260	400	4.5	3.5		31.3	58.9	51.0	27.0	1.9
3	0.591	8	167	74	76	170	-9040	-10100	775	1300	4.5	3.5		23.2	33.2	32.0	14.0	2.3
4	0.747	75	174	75	171	75	-1200	225	650	-2100	4.5	3.8		41.1	35.5	62.2	26.4	2.4
5	0.344	55	350	100	353	84	9240	-1200	-68000	-10500	4.5	3.5		70.9	70.9	118.7	71.1	1.7
6	0.856	52	172	84	171	85	-1300	-1750	1750	1000	4.6	3.8		71.9	53.7	82.0	19.1	4.3
7	1.079	35	20	329	326	20	-675	-625	-1650	-500	4.6	3.8		25.1	116.6	113.9	17.7	5.8
8	1.487	21	350	78	349	72	-240	-240	-260	40	4.6	3.8		21.8	49.4	52.4	19.6	2.7
9	1.373	30	172	78	172	74	-60	-800	260	-70	4.6	3.8		52.4	35.8	60.2	34.6	1.7
10	1.716	28	75	109	158	67	-580	50	230	-80	4.6	3.8		71.5	63.0	84.4	61.4	1.4
11	1.979	22	330	355	11	342	-90	-150	-180	-160	4.6	3.8		31.9	74.6	76.1	4.0	19.2
12	1.301	43	238	1	348	358	260	130	-300	-320	4.6	4.0		46.7	32.8	51.7	3.7	13.8
13	1.102	60	350	72	350	75	640	-220	-265	-470	4.6	4.0		54.1	28.8	54.5	28.0	2.0
14	1.035	79	349	80	75	348	480	55	-650	65	4.6	4.0		36.5	29.2	41.3	28.4	1.5
15	1.321	118	325	353	328	353	-60	40	170	140	4.6	4.0		22.3	19.0	23.2	10.9	2.1
16	1.119	99	173	180	175	180	-275	-350	-370	-300	4.6	4.0		57.3	52.8	60.8	7.4	8.2
17	1.396	82	355	35	6	353	350	290	-7	45	4.6	4.0		54.3	26.3	61.4	21.9	2.8
18	1.418	64	143	173	182	149	-360	-320	142	20	4.6	4.0		57.3	25.9	60.2	14.3	4.2
19	1.582	50	169	180	180	167	-250	-160	142	120	4.6	3.9		82.9	28.1	83.9	10.5	8.0
20	1.789	40	169	84	168	82	-45	-270	270	-105	4.6	3.9		50.2	75.0	84.2	50.4	1.7
21	2.193	31	171	76	75	170	90	-200	-65	165	4.6	3.9		53.6	75.1	77.6	46.2	1.7
22	2.328	25	14	101	94	10	-140	-90	20	-95	4.6	3.9		50.9	62.3	63.9	46.3	1.4
23	0.860	111	350	6	5	349	370	560	850	1075	4.6	3.8		30.6	41.9	53.1	29.9	1.8
24	1.103	129	349	89	349	77	-180	460	480	-40	4.5	3.8		30.0	39.5	46.5	29.4	1.6
25	1.487	137	289	211	295	203	-170	-15	50	-185	4.5	3.8		23.1	38.6	60.0	17.8	3.4
26	1.189	148	106	18	105	12	-350	-125	60	345	4.5	3.8		25.3	39.5	47.1	24.7	1.9
27	0.973	161	105	120	107	118	460	590	390	300	4.5	3.8		27.7	47.1	47.9	25.7	1.9
28	0.859	178	284	299	285	298	925	300	-460	-370	4.5	3.8		62.4	29.7	68.1	23.5	2.9
29	1.250	168	310	20	22	312	-950	-900	425	625	4.5	3.8		131.4	102.0	122.1	71.3	1.7
30	1.631	162	345	65	345	65	-250	-30	85	210	4.5	3.8		39.7	69.6	77.0	38.9	2.0
31	2.111	163	343	74	348	77	-130	-15	65	150	4.5	3.8		42.7	111.2	120.0	40.2	3.0
32	1.890	159	346	77	346	80	-180	45	60	160	4.5	3.8		46.7	86.0	107.6	29.4	3.7
33	2.112	144	139	246	140	246	110	-50	-10	-65	4.5	3.8		38.9	42.7	83.4	12.2	6.8
34	2.341	135	45	87	43	85	43	60	50	15	4.5	3.8		29.4	43.2	72.2	20.9	3.5
35	2.131	155	190	235	232	196	70	4	-110	-90	4.5	3.8		32.5	75.2	81.4	33.3	2.4

N	R	BEAR	B1	B2	BR1	BR2	EX1	EY1	EX2	EY2	CUR1	CUR2	XL	R1	R2	R_{max}	R_{min}	RTO
36	2.46	142	300	200	300	202	-40	-12	-20	-70	4.5	3.8	30	24.3	71.1	94.5	18.3	5.2
37	2.63	127	239	216	263	239	-45	-35	11	-7	4.5	3.8		40.5	40.7	85.6	12.0	7.1
38	0.43	176	183	99	92	181	8250	-850	1900	-1550	4.5	3.8		23.8	31.7	33.1	17.0	1.9
39	0.37	134	182	101	179	90	2900	8300	-4700	1800	4.5	3.8		23.6	31.2	41.3	14.4	2.9
40	0.32	351	171	181	170	180	-8000	-7700	1800	1150	4.5	3.5		26.1	34.1	62.9	1.8	34.8
41	2.46	163	40	53	61	46	-20	-12	130	120	4.55	3.8		22.5	134.8	151.7	7.1	21.5
42	2.71	171	227	244	229	244	-50	-80	-75	-85	4.55	3.8		79.9	120.9	147.4	8.5	17.3
43	1.13	196	55	140	149	58	-530	110	250	220	4.55	3.7		31.6	25.4	43.7	19.1	2.3
44	1.37	360	189	198	198	188	1150	1100	90	150	4.6	3.5		38.9	72.8	111.2	9.9	11.3
45	2.11	352	141	33	124	35	330	-300	100	10	4.5	3.5		66.3	73.7	77.5	53.9	1.4
46	1.71	354	342	68	342	72	-730	-35	-190	240	4.5	3.5		58.2	124.5	125.9	50.2	2.5
47	2.07	343	190	105	105	189	190	490	280	-60	4.5	3.5		81.5	210.1	212.2	40.7	5.2
48	2.43	347	189	205	205	188	120	28	-50	0	4.5	3.9		96.7	175.0	233.2	43.3	5.4
49	2.66	344	121	79	120	79	275	140	52	90	4.5	3.9		111.8	121.0	143.2	65.3	2.2
50	2.83	354	227	200	204	230	80	115	7	-25	4.5	3.8		59.4	108.7	115.5	10.0	11.5
51	2.96	348	281	255	281	255	90	12	-42	-35	4.5	3.8		99.1	77.4	151.3	13.8	10.9
52	3.1	357	127	65	126	66	65	-60	18	12	4.5	3.8		79.6	39.1	99.9	33.2	3.0
53	2.71	360	306	325	312	336	-145	-167	-48	-32	4.5	3.8		69.5	71.7	82.1	38.1	2.2
54	2.37	6	314	334	315	333	-130	-170	-90	-75	4.5	3.8		51.9	80.3	82.0	21.4	3.8
55	2.39	16	186	215	217	238	155	180	30	-28	4.5	3.8		55.7	119.7	125.2	19.4	6.4
56	2.36	339	114	129	100	116	140	170	90	60	4.5	3.7		53.5	130.6	143.8	45.5	3.2
57	1.25	313	168	81	172	77	950	1850	-145	220	4.5	3.7		92.6	27.8	91.5	3.3	27.6
58	1.73	318	145	55	145	57	300	360	-12	140	4.5	3.7		55.1	44.6	69.4	18.5	3.8
59	1.73	328	150	235	235	146	280	-430	-210	15	4.5	3.7		52.0	79.4	87.2	25.6	3.4
60	1.77	338	192	280	191	275	450	-80	70	90	4.5	3.5		44.0	50.9	53.2	34.5	1.5
61	1.39	330	93	6	80	6	1675	-350	480	220	4.5	3.7		75.0	100.8	104.5	57.3	1.8
62	2.61	331	202	101	198	84	80	250	-60	70	4.5	3.7		108.9	96.0	114.4	94.1	1.2
63	2.12	330	324	50	51	325	-140	130	100	-7	4.4	3.7		39.0	67.1	74.3	24.5	3.0
64	2.25	323	146	55	144	60	290	210	-10	105	4.4	3.7		97.0	76.8	123.4	38.7	3.2
65	2.84	325	174	80	173	80	110	120	-35	55	4.4	3.7		95.5	94.9	143.4	18.5	7.8
66	3.01	329	178	109	105	184	70	150	50	-35	4.4	3.7		96.9	121.9	157.5	55.7	2.8
67	1.45	190	345	9	8	346	-200	-240	-30	-80	4.5	3.7		29.4	25.6	44.7	13.8	3.2
68	2.19	183	77	159	77	160	-90	50	140	40	4.5	3.8		41.0	92.8	117.9	21.9	5.4
69	1.76	181	160	70	171	75	80	-175	3	170	4.5	3.7		38.9	62.8	81.9	19.2	4.3
70	1.46	206	126	35	14	112	-105	-200	-100	170	4.4	3.6		31.7	26.0	48.1	18.9	2.5

N	R	BEAR	B1	B2	BR1	BR2	EX1	EY1	EX2	EY2	CUR1	CUR2	XL	R1	R2	R_{max}	R_{min}	RTO
71	2.070	190	274	201	184	270	75	110	0	-90	4.4	3.7	30	39.4	44.8	72.0	23.2	3.1
72	1.798	206	359	90	2	97	-100	-170	-115	80	4.4	3.6		48.1	33.6	66.5	30.8	2.2
73	2.277	207	14	58	16	58	-37	-45	-10	8	4.4	3.65		21.6	12.4	21.9	8.8	2.5
74	2.798	210	90	129	85	165	-30	-12	0	15	4.4	3.65		35.3	14.0	37.7	14.1	2.7
75	2.972	195	229	322	322	228	35	5	-30	-10	4.4	3.65		33.8	44.8	71.5	23.2	3.1
76	1.798	194	80	169	167	80	-130	72	65	120	4.4	3.7		34.0	41.6	65.6	20.2	3.2
77	2.333	194	200	218	194	213	80	100	0	-20	4.4	3.65		52.5	41.0	56.0	19.7	2.8
78	1.158	234	283	17	282	18	320	-35	-20	-620	4.4	3.7		28.0	21.1	36.8	20.2	1.8
79	1.554	225	170	185	170	185	7	30	140	170	4.4	3.7		16.4	21.2	22.2	2.9	7.7
80	1.216	254	263	168	279	175	85	-170	480	300	4.4	3.7		21.6	22.3	28.6	19.9	1.4
81	1.570	251	6	302	350	4	75	100	-30	-60	4.4	3.7		25.1	12.0	35.4	9.03	3.9
82	1.603	235	352	264	353	262	50	85	-100	80	4.4	3.7		21.5	13.4	28.6	13.3	2.1
83	0.396	253	72	87	86	72	-1735	-2300	12000	12000	4.6	3.5		24.2	13.5	25.8	2.3	11.1
84	0.732	248	318	194	184	270	900	140	2900	4000	4.4	3.6		37.9	12.9	42.5	12.9	3.3
85	1.011	213	130	233	230	144	-260	725	90	480	4.4	3.6		37.4	17.5	43.0	18.0	2.4
86	0.786	275	172	80	175	83	-875	140	-1150	-675	4.3	3.7		33.6	11.0	75.6	2.5	29.6
87	0.643	313	260	271	258	272	-2025	-1600	-900	-775	4.3	3.7		25.2	21.7	120.2	17.8	6.7
88	1.109	287	51	75	60	82	460	410	60	-120	4.3	3.7		33.5	18.9	32.7	10.1	3.2
89	1.414	272	342	245	348	230	140	-65	85	180	4.3	3.7		26.4	17.9	38.3	5.2	7.4
90	1.707	267	175	81	170	83	-100	35	0	-115	4.3	3.7		32.4	14.7	36.5	13.2	2.8
91	1.807	242	200	128	128	203	13	-65	5	80	4.3	3.7		24.6	13.0	34.5	11.5	3.0
92	1.911	231	97	174	175	95	-70	-15	65	-40	4.3	3.7		24.8	17.1	28.3	17.2	1.6
93	2.414	217	125	197	126	199	-25	15	10	13	4.3	3.7		21.1	7.5	31.7	6.2	5.1
94	2.012	216	7	265	6	231	-15	85	-45	55	4.4	3.7		30.5	16.3	33.1	15.4	2.1
95	1.783	284	139	205	138	192	-15	-155	-120	-90	4.4	3.75		44.4	21.8	46.1	18.5	2.5
96	2.286	305	81	173	82	173	190	-20	30	-40	4.4	3.75		69.0	27.1	80.0	19.2	4.2
97	2.012	297	352	295	357	311	100	-145	60	60	4.4	3.75		76.5	21.4	76.9	1.9	40.2
98	2.752	312	31	85	31	85	45	110	50	32	4.4	3.70		67.0	54.0	97.0	22.8	4.2
99	3.048	318	340	53	68	343	-45	35	30	45	4.4	3.70		45.3	88.2	114.3	2.5	45.5
100	2.347	314	175	281	180	276	15	-175	-60	-50	4.4	3.75		61.1	57.2	84.3	35.3	2.4
101	1.979	306	12	348	334	354	125	48	65	85	4.4	3.75		48.1	34.4	63.7	7.4	8.6
102	1.774	300	300	215	213	310	-175	-250	-65	40	4.4	3.75		55.6	16.7	60.1	1.2	48.9
103	1.518	284	286	190	286	175	-70	-180	100	-100	4.4	3.75		34.9	12.7	35.0	12.7	2.8

APPENDIX A-3

TEMPERATURE STUDY FIELD DATA

N: Station number

R: Resistance (ohms)

T: Temperature (^{o}C)

N	R	T	N	R	T
1	972	25.8	36	952	26.3
2	920	27.3	37	955	26.2
3	1009	24.8	38	921	27.2
4	933	26.9	39	983	25.5
5	1007	24.8	40	950	26.4
6	961	26.1	41	977	25.6
7	943	26.6	42	966	25.9
8	889	28.2	43	970	25.8
9	979	25.6	44	954	26.3
10	977	25.6	45	971	25.8
11	959	26.1	46	947	26.5
12	1016	24.6	47	952	26.3
13	973	25.7	48	970	25.8
14	966	25.9	49	971	25.8
15	1015	24.6	50	959	26.1
16	1005	24.9	51	1000	25.0
17	965	26.0	52	1010	24.7
18	998	25.1	53	961	26.1
19	982	25.5	54	951	26.4
20	989	25.3	55	975	25.7
21	1027	24.3	56	960	26.1
22	978	25.6	57	989	25.3
23	999	25.0	58	1313	17.7
24	993	25.2	59	989	25.3
25	988	25.3	60	974	25.7
26	998	25.0	61	996	25.1
27	988	25.3	62	997	25.1
28	1014	24.6	63	978	25.6
29	947	26.5	64	960	26.1
30	1022	24.4	65	935	26.8
31	984	25.4	66	927	27.1
32	945	26.5	67	930	27.0
33	958	26.2	68	972	25.8
34	949	26.4	69	962	26.0
35	953	26.3	70	1022	24.4

APPENDIX A-4

SELF-POTENTIAL STUDY FIELD DATA

N: Station number

V: Potential drop along a 200 m line (millivolts)

V_C: Corrected value of V (after error distribution) (millivolts)

V_N: Potential drop between a station and the initial point with assumed zero potential (millivolts)

N	V	V_C	V_N
1	-23.9	-21.9	-21.9
2	-33.4	-31.4	-53.3
3	- 6.2	- 4.2	-57.5
4	- 7.9	- 5.9	-63.4
5	-27.7	-25.7	-89.1
6	24.5	26.5	-62.6
7	-54.5	-52.7	-115.3
8	- 2.9	- 0.9	-116.2
9	-13.2	-11.2	-127.4
10	-24.6	-22.6	-150.0
11	8.0	10.0	-140.0
12	-19.6	-17.6	-157.6
13	- 4.7	- 2.7	-160.3
14	- 9.9	- 7.9	-168.2
15	0.2	2.2	-166.0
16	-12.8	-10.8	-176.8
17	- 3.1	- 6.1	-182.9
18	- 7.7	- 5.7	-188.9
19	-11.3	- 9.3	-197.9
20	-31.0	-29.0	-226.9
21	5.2	7.2	-219.7
22	- 8.4	- 6.4	-226.1
23	-32.2	-30.2	-256.3
24	- 5.8	- 3.8	-260.1
25	-16.1	-14.1	-274.2
26	- 4.8	- 2.8	-277
27	- 1.5	0.5	-276.5
28	- 7.8	- 5.8	-282.3
29	-15.9	-13.9	-292.2
30	-24.0	-22.0	-318.2
31	-40.0	-38.0	-356.2
32	-30.8	-28.8	-385.0
33	-15.1	-13.1	-398.1
34	3.8	5.8	-392
35	-20.2	-18.2	-410.
36	-1.4	0.6	-225.
37	10.8	12.8	-214.7
38	- 2.7	- 0.7	-215.4
39	10.8	12.8	-202.
40	12.7	14.7	-187.9
41	13.4	15.4	-172.5
42	8.1	10.1	-162.4
43	18.5	20.5	-141.9
44	8.3	10.3	-131.6
45	11.2	13.2	-118.4
46	30.8	32.8	- 75.6
47	-30.0	-28.0	-103.6
48	- 1.0	1.0	-102.6
49	43.2	45.2	- 67.4
50	- 2.7	- 0.7	-258.0
51	27.3	29.3	-228.7
52	-12.0	-10.0	-238.7
53	6.8	8.8	-229.9
54	1.6	3.6	-226.3
55	0.8	2.8	-222.5
56	- 0.8	1.2	-221.3
57	10.6	12.6	-208.7
58	-10.2	- 8.2	-216.9
59	- 8.9	- 6.9	-223.8
60	0.3	2.3	-221.5
61	- 3.4	- 1.4	-222.9
62	0.1	2.1	-220.8
63	-19.0	-17.0	-237.8
64	- 4.0	- 2.0	-239.8
65	6.0	8.0	-231.8

REFERENCES

Banwell, C. J., 1970, Geophysical techniques in geothermal exploration: UN Symposium on the Development and Utilization of Geothermal Resources, Pisa, 1970, sec. IV.

Dedkova, D., Halousek, J., Krcmar, B., and Prihoda, K., 1970, Geothermal prospection in shallow holes and its limitation: UN Symposium on the Development and Utilization of Geothermal Resources, Pisa, 1970, IV/5.

Furgerson, R. B., 1970, A controlled-source telluric current technique and its application to structural investigations: Thesis 1313, Colo. School of Mines, Golden, Colo.

Furgerson, R. B., and Keller, G. V., 1974, Computed dipole resistivity effects for an earth model with vertical and lateral contrasts in resistivity: Report No. NR081275, Office of Naval Research, Washington, D.C.

Grose, L. T., and Keller, G. V., 1974, The Colorado School of Mines Nevada Geothermal Study - Report of Progress for the period May 1, 1974 to July 31, 1974: Colo. School of Mines, Golden, Colo.

Jordan, J. M., 1974, Geothermal investigations in the San Luis Valley, South-Central Colorado: Thesis 1478, Colo. School of Mines, Golden, Colo.

Keller, G. V., 1974, Drilling at the summit of Kilauea Volcano: Prepared for National Science Foundation, Colo. School of Mines, Golden, Colo.

_____ 1966, Dipole method for deep resistivity studies: Geophysics, v. 31, no. 6, p. 1088-1104.

_____ 1970, Induction methods in prospecting for hot water: Geothermics, spec. issue 2, p. 318-332.

Macdonald, G. A., and Abbott, A. T., 1970, Volcanoes in the sea, the geology of Hawaii: Honolulu Hawaii, University of Hawaii Press.

Stearns, H. T., 1966, Geology of the State of Hawaii: Palo Alto, Calif., Pacific Books.

Strange, W. E., Woollard, G. P., and Rose, J. C., 1965, An analysis of the gravity field over the Hawaiian Islands in terms of crustal structure: Pacific Sci., v. 19, no. 3, p. 381-389.

Van Nostrand, R. G., and Cook, K. L., 1966, Interpretation of resistivity data: U.S. Geol. Survey Prof. Paper 499.

APPENDIX B

EXPLORATION ON ADAK ISLAND, ALASKA

by

David L. Butler and George V. Keller

Appendix B accompanies a report entitled "Geothermal Energy in the Pacific Region" by L. T. Grose and G. V. Keller, May, 1975. This project has been supported by the Office of Naval Research Contract Number N00014-71-A-0430-0004.

APPENDIX B - EXPLORATION ON ADAK ISLAND, ALASKA

David L. Butler and George V. Keller

Introduction

As pointed out in the body of this report, the Aleutian Islands comprise an area of active to recently active volcanism which should be favorable for the occurrence of geothermal energy. Adak Naval Base is an excellent candidate for the use of geothermal energy, inasmuch as Adak Island is located toward the western end of the active portion of the Aleutian Islands. Because of this, some exploration was carried out on Adak Island in an attempt to evaluate the geothermal potential. Seismicity and resistivity surveys were carried out on Mount Adaydak, on northern Adak, near the Naval Base (see Figure 1).

The area of interest, the northern mountainous part of Adak, is the remnants of three historically inactive volcanoes. From east to west, the volcanoes are Mount Adagdak, Andrew Bay Volcano, and Mount Moffet. Although no extensive faulting has been mapped in this area, some evidence of faulting is present on the north slope of Mount Adagdak. The lithology of this area includes volcanic and intrusive rocks of Paleozoic age, Tertiary to Quaternary volcanic rocks and Quaternary alluvium. The alluvium unit consists largely of glacial drift and other unconsolidated materials, including volcanic ash.

Seismicity Surveys

More than 1000 km^2 near Adak Island was surveyed from Oct. 22 to November 1, 1974, for microearthquakes to aid in the evaluation of the geothermal potential of the area. The survey was carried

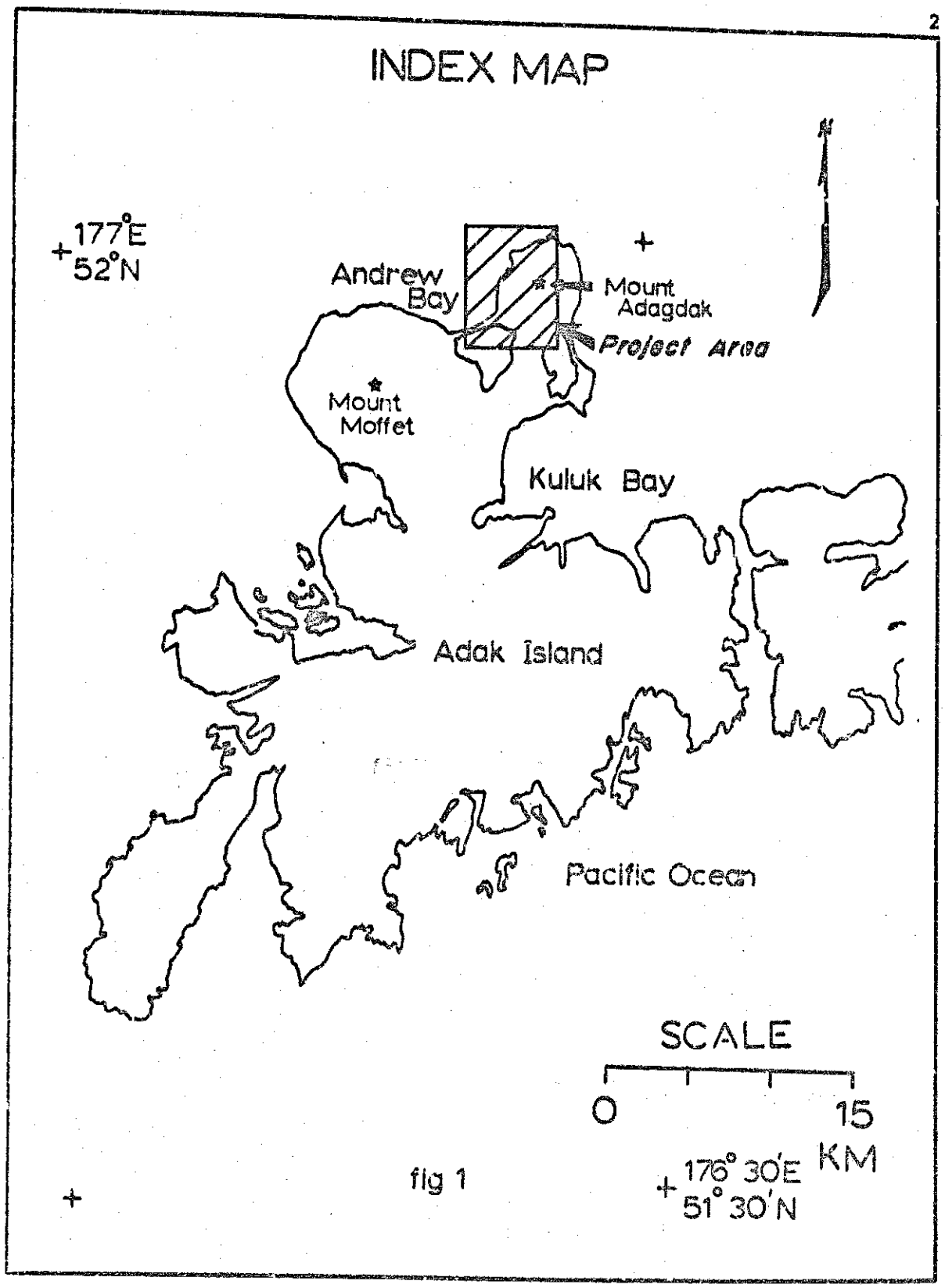
INDEX MAP
177°E
52°N
Andrew Bay
Mount Adagdak
Project Area
Mount Moffet
Kuluk Bay
Adak Island
Pacific Ocean
SCALE
0
15
KM
176° 30'E
51° 30'N

fig 1

out by Microgeophysics, Inc., under contract to the Colorado School of Mines. The size of the 1000 km^2 area is based on a detection threshold of magnitude 0 or less with at least one station recording an event within the area. The objective was to detect and locate microearthquakes and thereby map tectonically active structures.

Figure 2 is an historical seismicity map of the area around the Adak Island. The Aleutian Arc is an active seismic province, however, a large number of the events shown on Figure 2 occur on or near the subduction or Benioff Zone of the Aleutian Island arc-trench system. The subduction zone is the postulated tectonic feature occurring where one crustal plate is being forced under another. In the Aleutian Islands, the North Pacific Plate is being moved in a northwesterly direction under the American Plate.

The subduction zone strikes east-west south of Adak and dips to the north to a depth of 100 to 150km beneath the island. The seismic activity associated with the subduction zone occurs at too great a depth to be of interest in this survey but the tectonic activity at depth is a manifestation of the regional stress. This same stress pattern may influence surface faulting and the shallow microseismicity of interest in this survey.

The specific project area contains no historical epicenters although several epicenters are northeast of the area of interest. In early March, 1974, 13 small earthquakes were detected by the NOAA Seismological Observatory on Adak and located near Andrew Bay and Mount Adagdak (Mr. D. Glover, personnel communication, 1974). These events are of small magnitude ($m<3$) and are not plotted on the historical seismicity map (Figure 2).

HISTORICAL SEISMICITY

fig 2

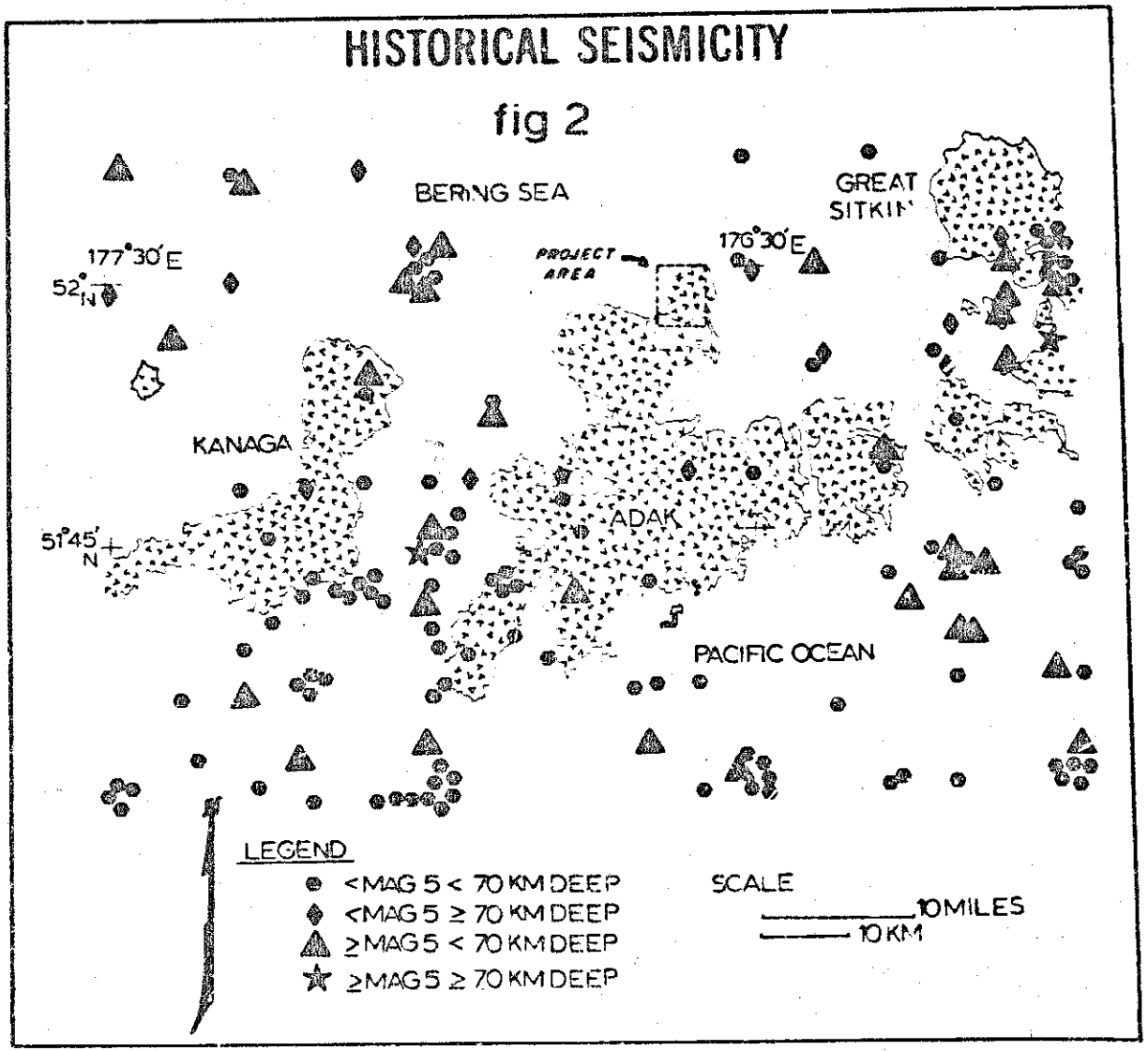

During the course of this survey, assistance and data were supplied by Mr. D. Glover, observatory director of the National Oceanic and Atmospheric Administration (NOAA), Seismological Observatory, Adak, Alaska. The data supplied includes arrival times, S-P times and magnitudes of several local earthquakes. His enthusiastic assistance is gratefully acknowledged.

The next section of this paper outlines the instrumentation and operational methods employed in the field work. The observations and analysis are given in a section and are followed by an interpretation of the results. Recommendations are listed in the last section of the body of the report. The appendix is a listing of times, locations and magnitudes of the local earthquakes detected during this survey.

Instrumentation and Operational Summary

Seven Sprengnether Instrument Co. MEQ-800-B portable seismic systems were used for this survey. Each system consists of a Mark Products model LC-4, 1-hz natural-frequency vertical seismometer, gain-stable amplifier, integral timing system, and smoked paper recording with 0.025mm stylus width and 120mm/min recording speed. The frequency characteristics of the instrument are summarized in Figure 3 (note that both the velocity response and the displacement response are plotted; displacement response at a particular frequency, f, is obtained by multiplying the velocity response by $2\pi f$). Gain changes are by 6db steps from the typical operating level of +96db plotted in the figure.

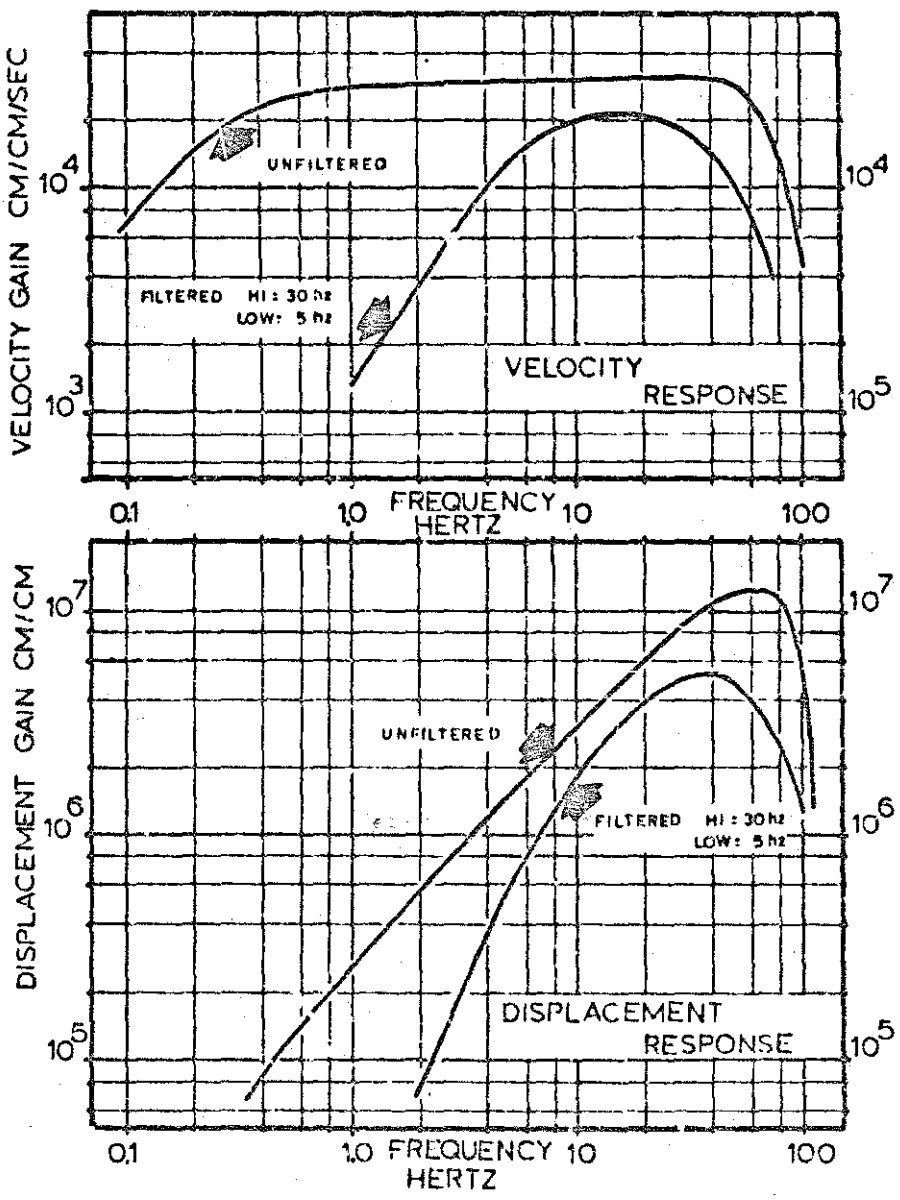

INSTRUMENT RESPONSE

fig 3

INSTRUMENT RESPONSE IS PLOTTED FOR 96db GAIN

Clocks were synchronized daily with a master clock, which was synchronized with WWV. Clock drifts between synchronizations were below expected record reading errors, therefore no corrections were necessary. Records were read to $\pm$0.03 sec for P arrivals and $\pm$0.10 sec for S-P times. Amplitudes, peak to peak, were read to the nearest millimeter, and durations to the nearest 0.5 sec.

Despite the poor working conditions, considerable effort was made to locate stations on hardrock outcrops (crystalline exposures or well compacted sediments). All stations were operated at the gain limit allowed by ambient background noise. Station locations of the array operated for ten days are illustrated in Figure 4 and listed in Table 1. Stations 1 through 9 were operated by MicroGeophysics Corporation; z1-z5 and AD8 by NOAA. Details of the operation of stations 1 through 9 are shown in Table 2. The NOAA stations, which are operated continuously, are part of the permanent tsunami-warning network of NOAA. The operation schedule (Table 2) shows the gains and the time periods of individual station occupations.

MAP OF STATION LOCATIONS

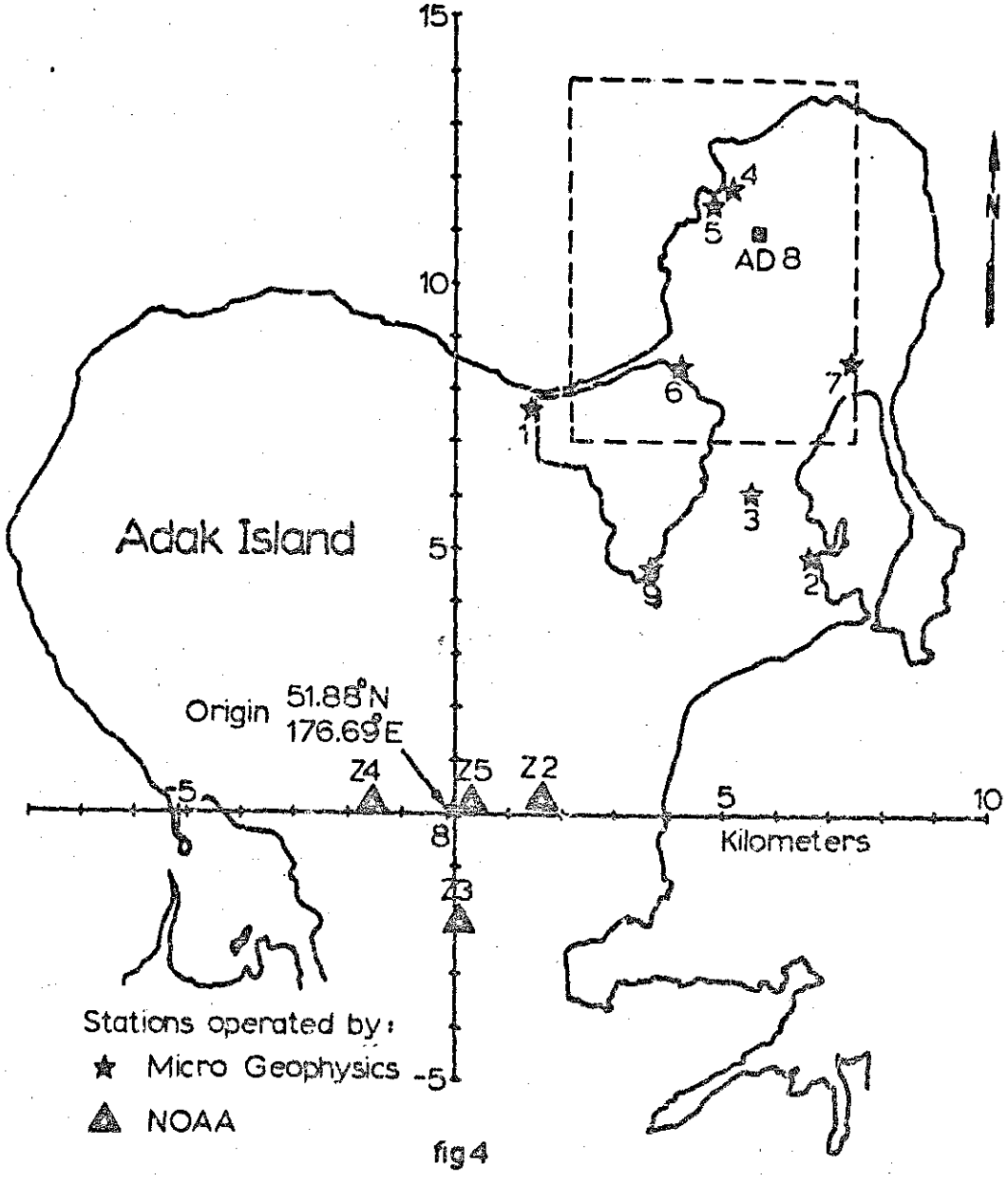

fig 4

STATION COORDINATES

TABLE 1

Station	X* in km	Y* in km	Z* in km
1	1.33	7.60	0.00
2	6.62	4.95	0.00
3	5.38	6.03	0.03
4	5.15	11.75	0.09
5	4.80	11.40	0.09
6	4.15	8.42	0.03
7	7.31	8.58	0.05
8*	0.00	0.00	0.09
9	3.70	4.60	0.03
z2	1.70	0.35	0.06
z3	0.05	-1.90	0.03
z4	-1.60	0.15	0.09
z5	0.15	0.05	0.09
AD8	5.60	11.00	0.24

* The origin is located at station 8 (latitude 51.88°N, longitude 176.69°W). Positive X and Y are east and north respectively.

Z is the station height above sea level (altitude).

OPERATION SCHEDULE

table 2

g.12 = gain/one million at 20 Hertz

filters at 5-30 Hz

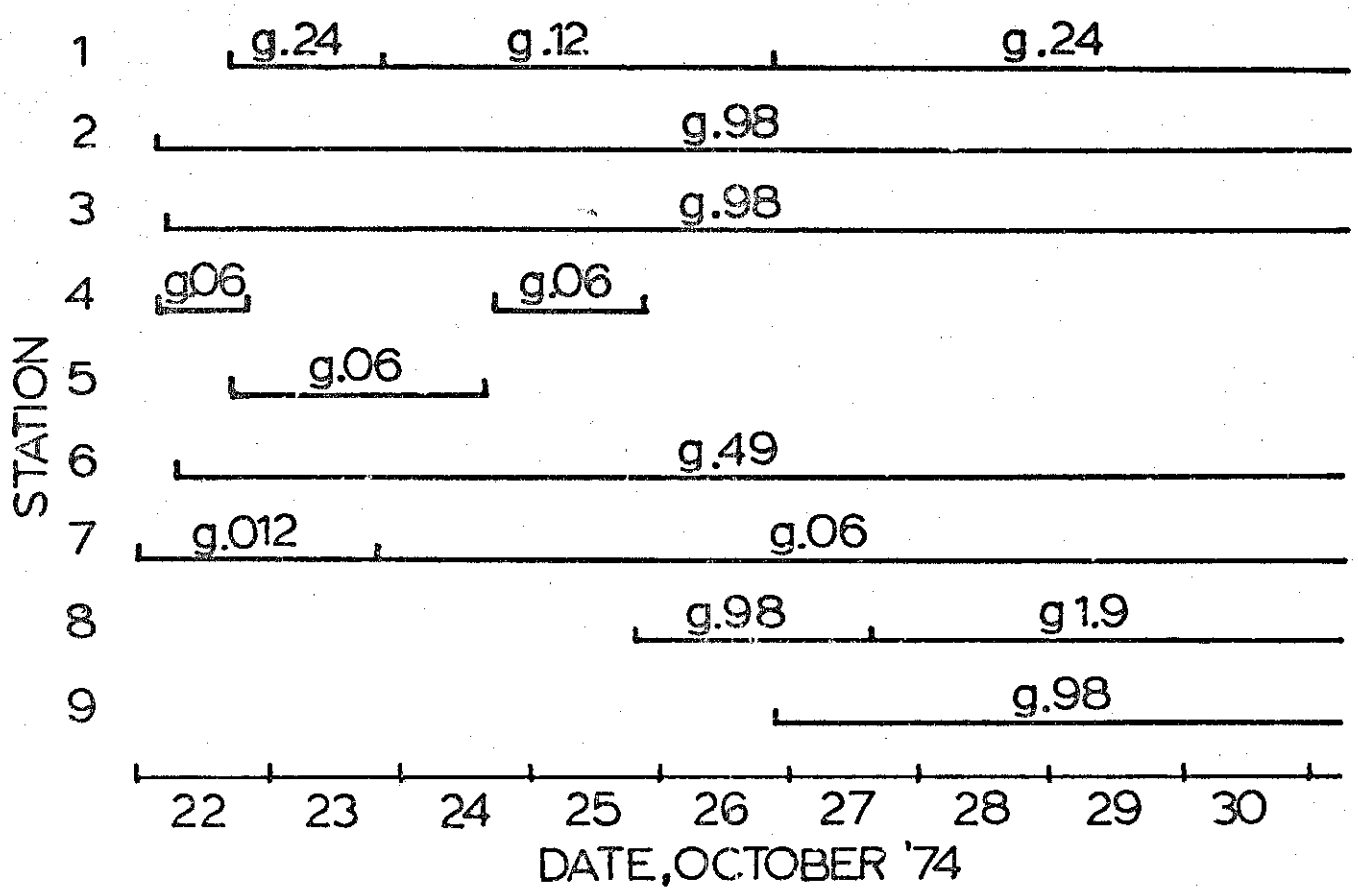

Observations and Analysis

Events were regarded as seismic in origin if they appeared on two or more stations with time differences corresponding to seismic velocities or if they were similar in appearance to other larger events which were well recorded. Seismic events were considered local if they had S-P times of less than four seconds.

The S-P time is a characteristic indicator of distance to the epicenter of an event. The S-P time is the difference between the arrival time of the S or shear wave and the P or compressional wave. The two body waves propagate by different mechanisms and at different velocities dependent on the parameters of the transporting medium. The S-P time is thus a function of the distance traveled.

An example of a local event near Adak is shown in Figure 5. Regional and teleseismic (distant) events with S-P times greater than four seconds, were considered outside the scope of this survey and therefore no attempt was made to locate them. The four-second S-P time cut-off for local events is an arbitrary limit chosen by the interpreter.

Local events timed on four or more stations were located using a generalized inverse computer program. This program assumes a velocity model and least-squares fits calculated travel times to the observed arrival times. The velocity structure in the project area can be estimated from a layered crustal velocity model of the Adak region developed by the USGS (Engdahl, 1974). Figure 6 illustrates the USGS model and two

EXAMPLE OF A LOCAL EVENT

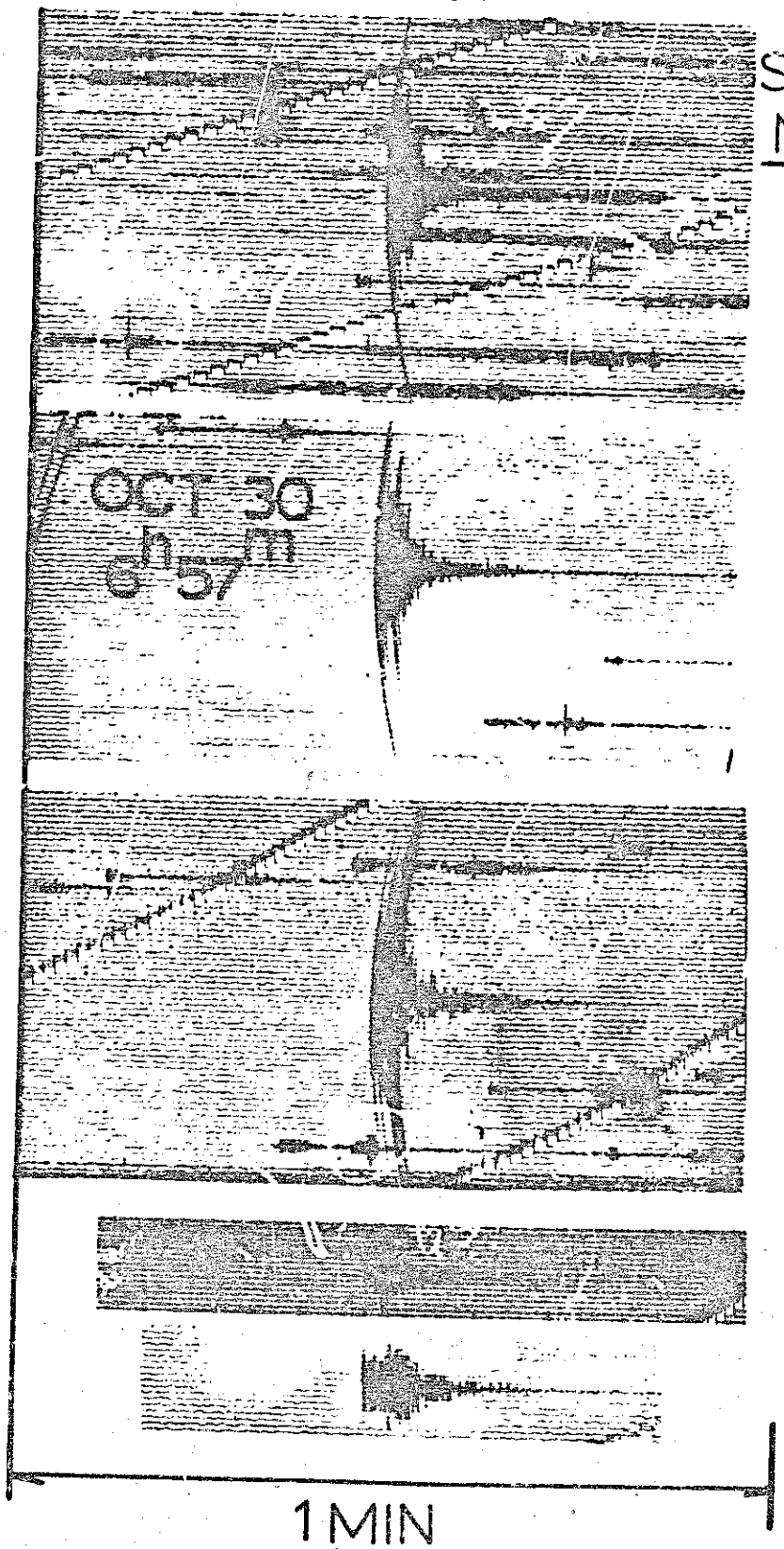

fig 5

VELOCITY STRUCTURE MODELS

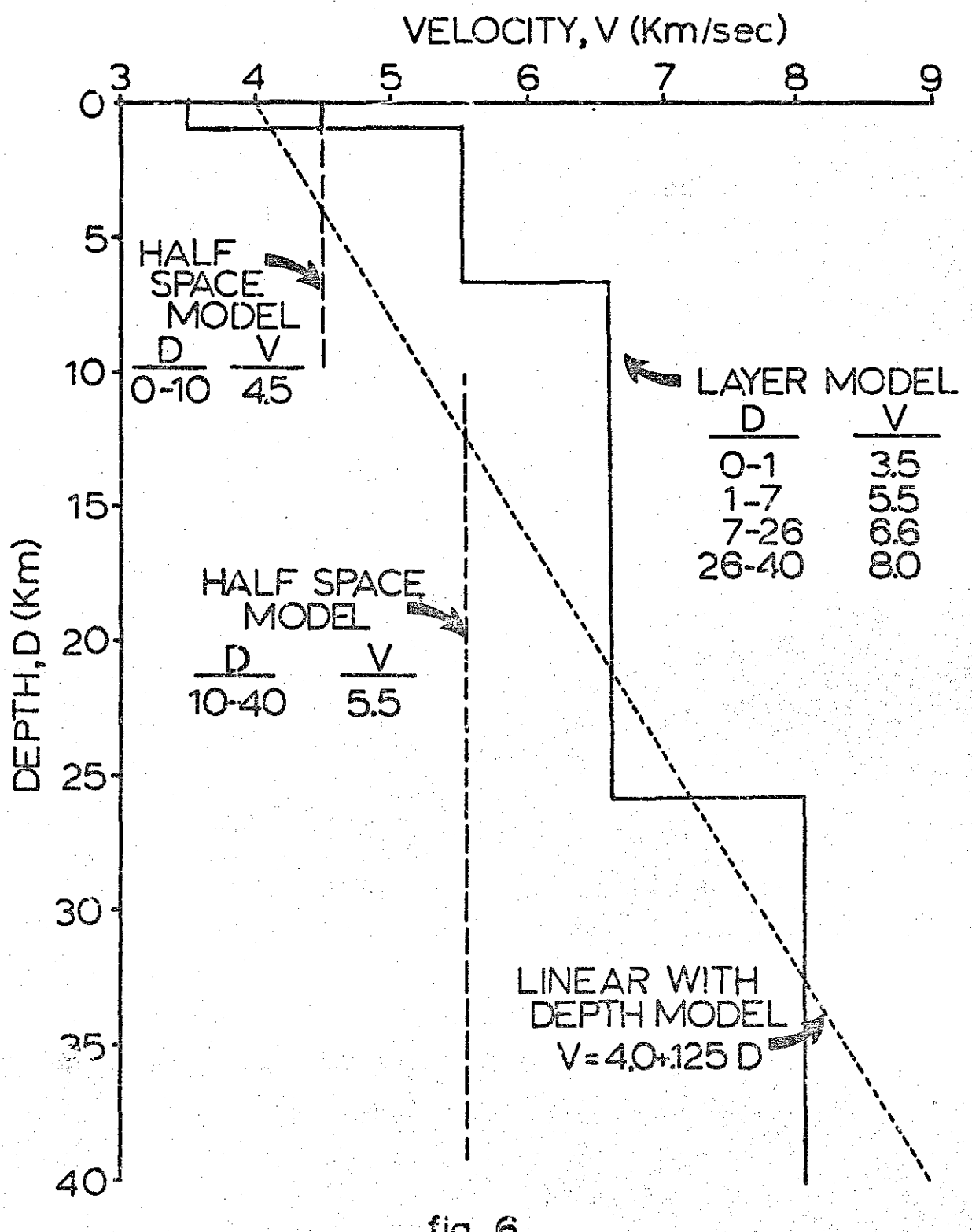

fig 6

other velocity structures, a half-space model and a linear velocity-increase-with-depth model. The half-space model was used to test the picked arrival times and the sensitivity of the locations to velocity changes. The constant velocity model obtained good fits with no anomalous station residuals. The velocities obtained with the half-space model agree with the averaged velocities of the layered model. The model that produced the best fits and lowest residuals in the project area was the linear velocity-increase-with-depth model. This model is in general agreement with the layered model and it produced station residuals on the order of the picking error (±.03 sec).

Figure 7 shows all located events and illustrates that the local seismicity is confined to two areas. Events from these two areas were identified by using S-P times and signature similarities and were classified as "type A" or "type B" events. Figure 8 shows a plot of the cumulative number of events recorded during the survey of each type. Type A events were recorded at a rate of four events per day, type B events at a rate of three per day when there was activity.

Type B events were located 30 to 40km southeast of Adak. Due to the distance from the array, the epicenter location precision is about ±4km. Because these events are well outside the area of interest, no further analysis was performed.

Twenty six events denoted as type A were located in the project area. The precision of location for these events is about ±1km in plan and ±2km in depth. The events occur within

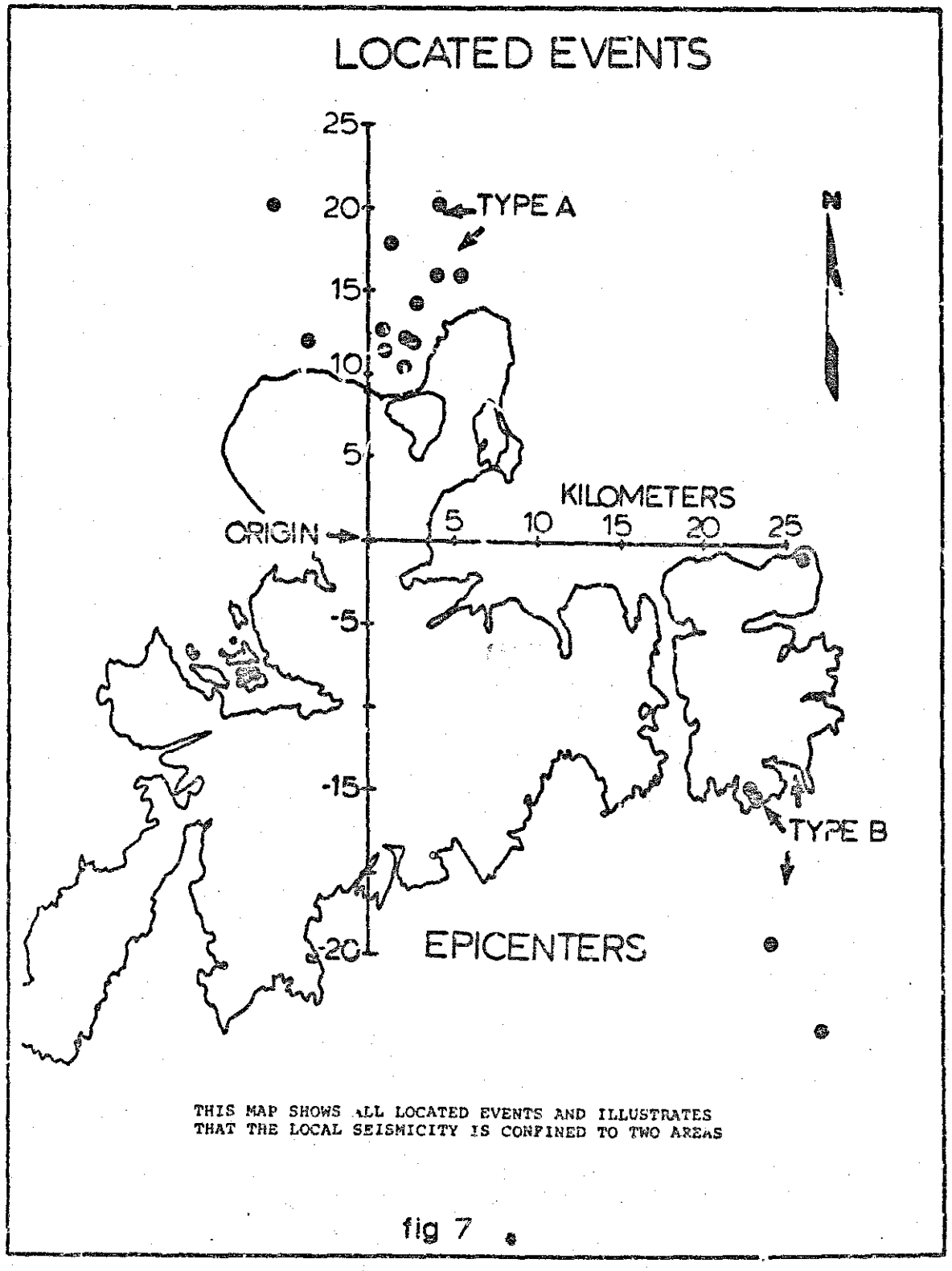

THIS MAP SHOWS ALL LOCATED EVENTS AND ILLUSTRATES
THAT THE LOCAL SEISMICITY IS CONFINED TO TWO AREAS

fig 7

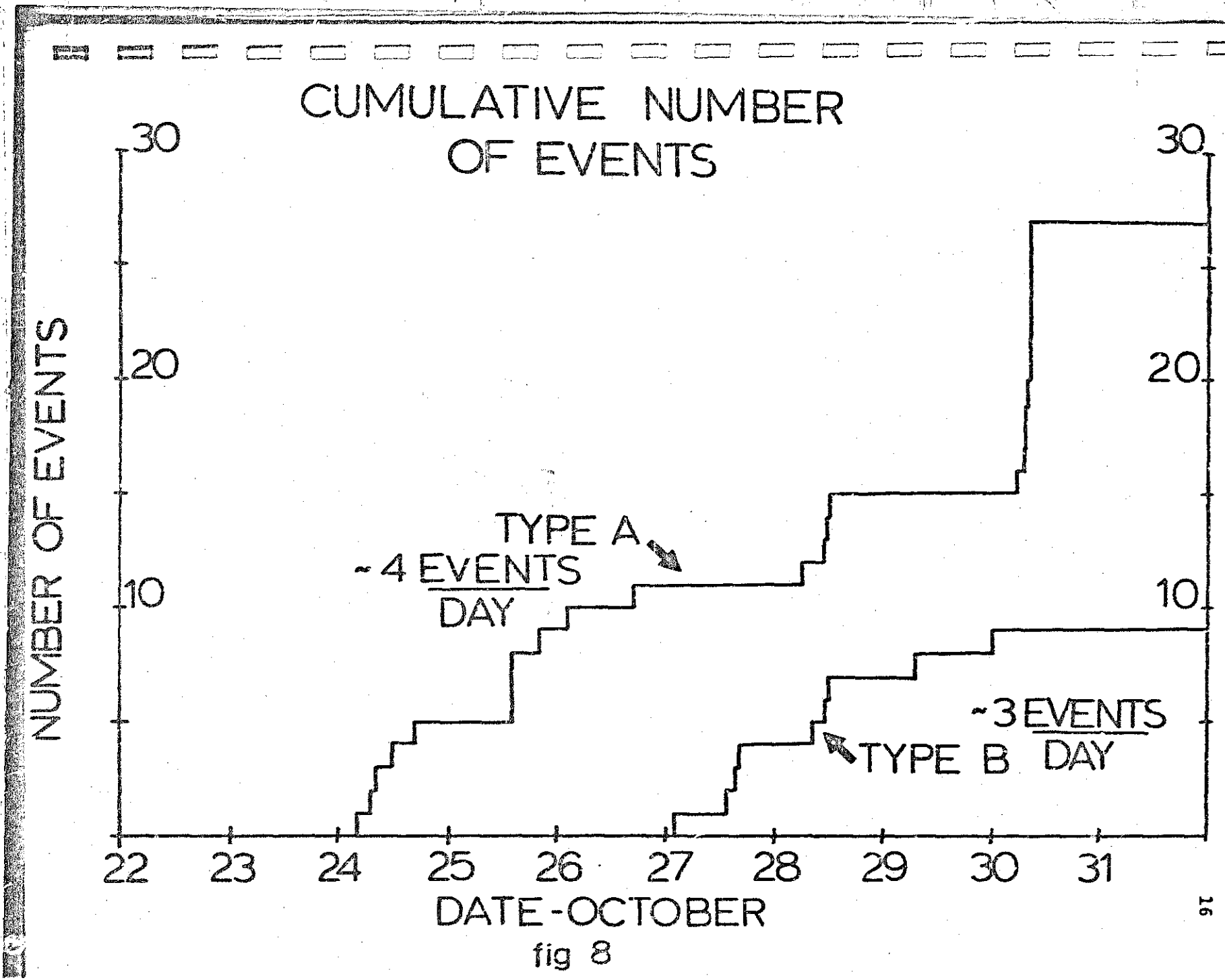
CUMULATIVE NUMBER
OF EVENTS
NUMBER OF EVENTS
30
20
10
TYPE A
~4 EVENTS
DAY
~3 EVENTS
DAY
TYPE B
22
23
24
25
26
27
28
29
30
31
DATE-OCTOBER

fig 8

Andrew Bay, west and northwest of Mount Adagdak. The located type A events are shown in Figure 9. The least-squares-fit fault plane of the event location is shown in Figure 10. The least-squares-fit solution is arrived at in the following manner. After the surface fault trace is plotted in plan view, an auxilary or cross section view is taken perpendicular to the strike of the fault trace (to show the true dip of the fault plane). The depth perspective of the fault is found by plotting the depths of epicenters (hypocenters) in the auxilary view. After allowing for uncertainties in the depth parameter from the velocity model ($\pm$2km), a fault plane can be fitted to the cross section. The fault plane strikes N60°E and dips NW at 70°. The dotted line is the expected precision of the fault plane solution.

The direction of movement on the fault plane is obtained by the use of a first motion study. This solution is shown on Figure 11. The first motion, compression for vertical motion up and dilatation for vertical motion down, is plotted on the upper hemisphere of a sterographic projection. A fault plane is then fitted to the data by dividing the plot into four quadrants. The shaded region on Figure 11 represents compression and the unmarked region represents the dilatation quadrants. The first-motion method produces two orthogonal solutions. If you chose the fault plane solution which strikes N70°E with a NW dip of 75° the relative motion of the fault is right-lateral, strike-slip with a small component of thrust. The fault plane

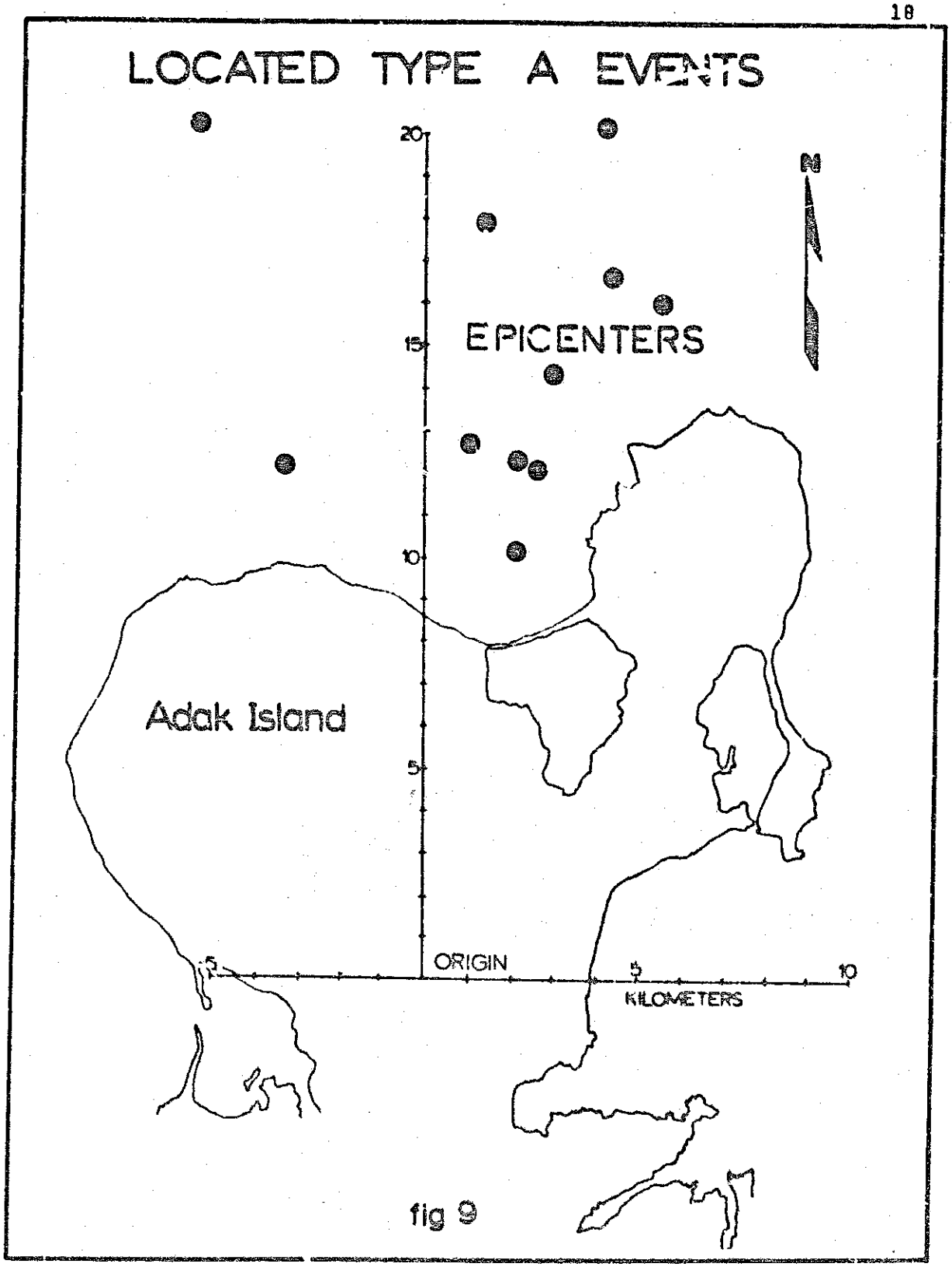
LOCATED TYPE A EVENTS
EPICENTERS
N
20
15
10
5
Adak Island
ORIGIN
5
10
KILOMETERS

fig 9

LEAST SQUARES FIT FAULT PLANE SOUTION

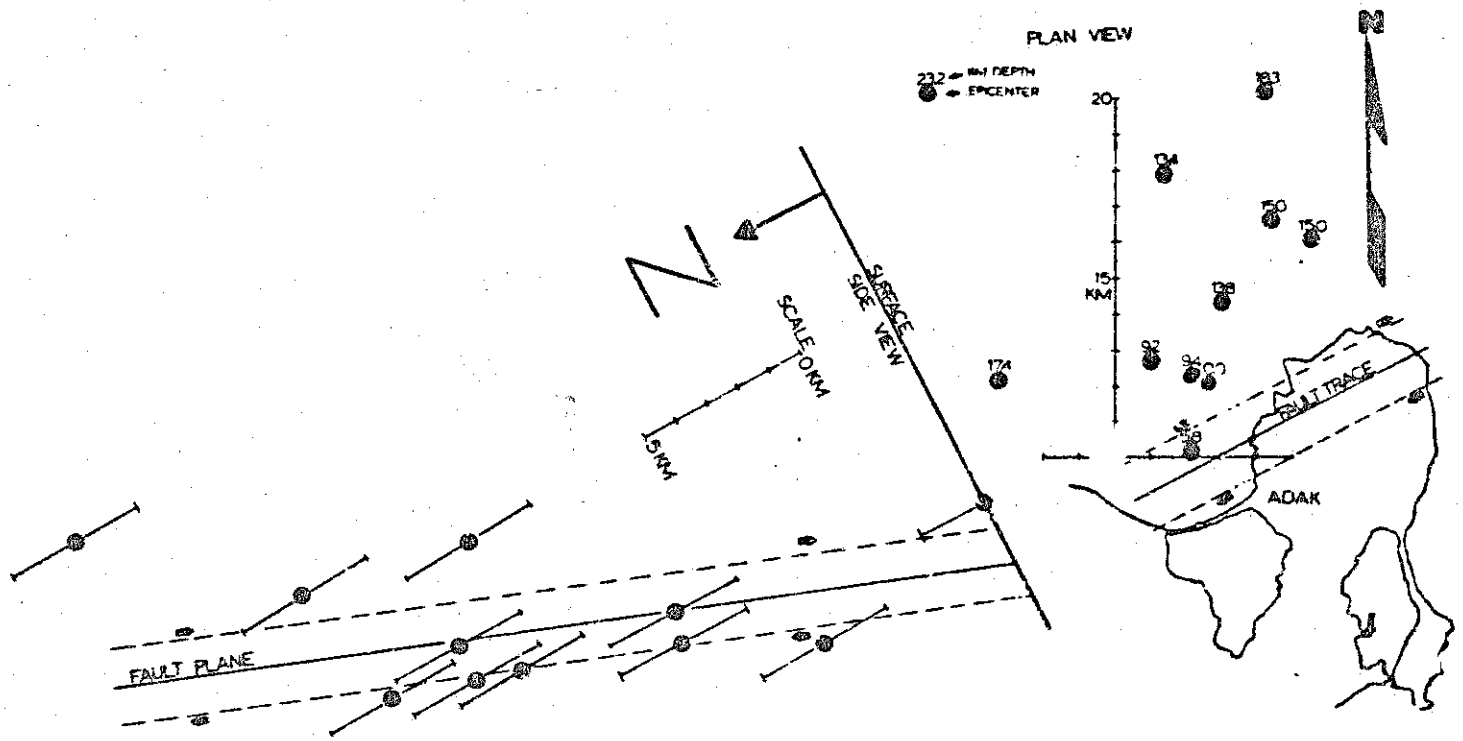

fig 10

AUXILIARY CROSS SECTION IS CONSTRUCTED NORMAL TO STRIKE OF FAULT TRACE. DEPTHS OF HYPOCENTERS ARE PLOTTED (WITH ALLOWED ERROR) AND LEAST SQUARE FIT SOLUTION TO FAULT PLANE IS DRAWN.

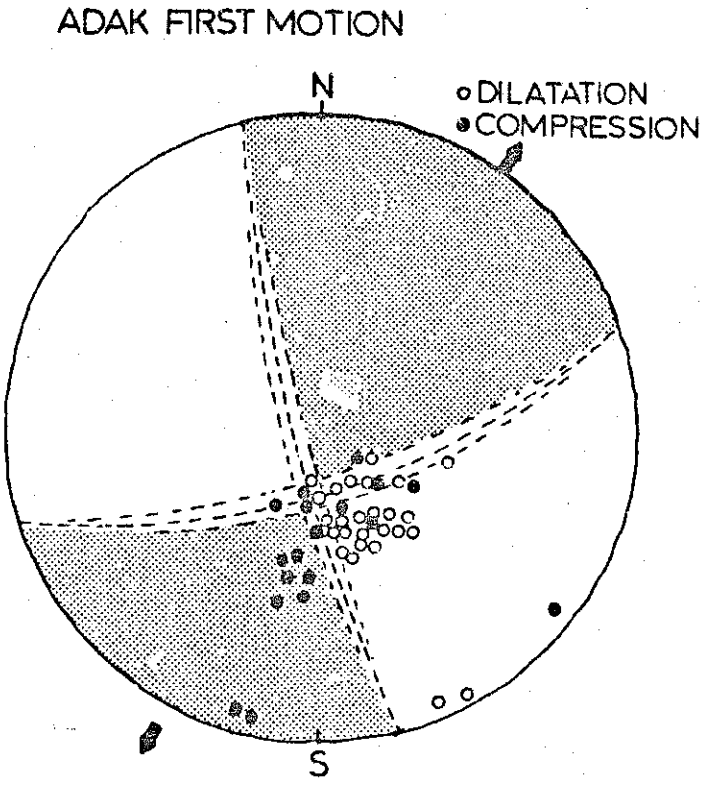

fig 11

solutions from the two methods agree well within reasonable limits of accuracy.

To estimate the level of seismicity some attention must be paid to the size or magnitude of an earthquake. In this survey an amplitude versus distance plot (see Figure 12) was constructed for two local events (October 30 at 6^h57^m and at 8^h15^m). The magnitude of these events was determined by using curves established for microearthquakes

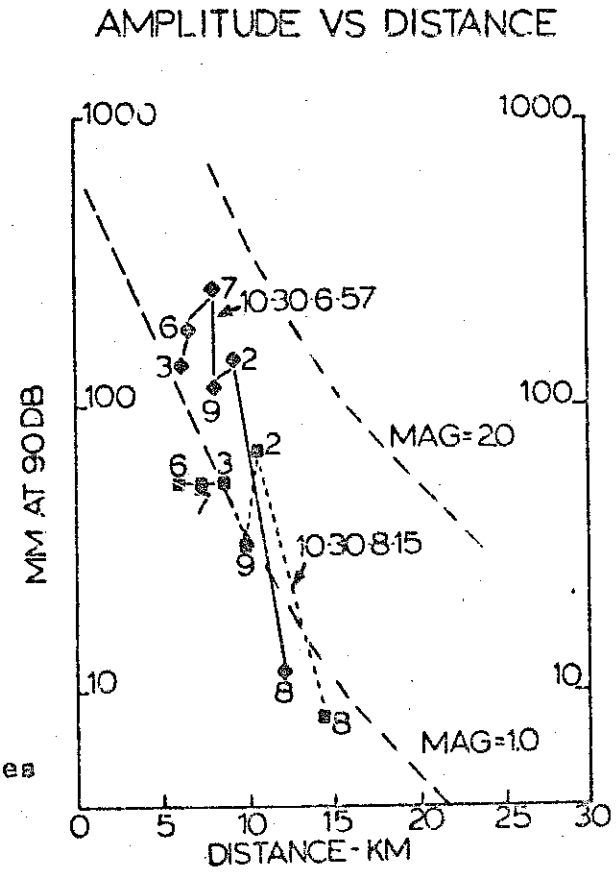

fig 12

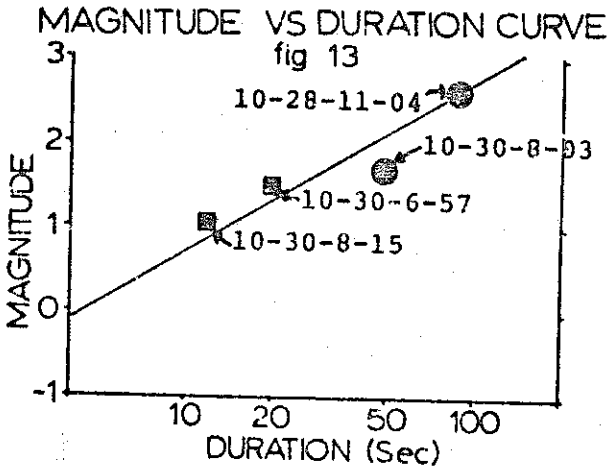

by Brune and Allen (1967). Magnitudes from two other larger events (October 28, 11^h04^m and October 30 at 8^h03^m) were supplied by the NOAA Adak Observatory. These four events were then used to determine a magnitude versus duration curve (see Figure 13). To correct for local geologic effects all durations were measured at station 3.

From the magnitude versus duration curve, all detected events were assigned a magnitude. The resulting cumulative recurrence curve (a plot of the log of the number of events of a given magnitude versus the magnitude) is shown in Figure 14.

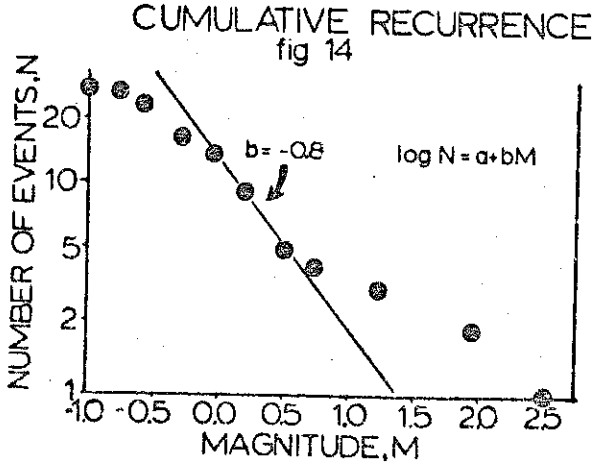

The slope of this linear relationship is often called the b-slope. A b-slope of -0.8 is shown with the data for reference.

Figure 15 shows the relationship between Poisson's ratio and the velocity ratio . The often assumed value of Poisson's ratio of 0.25 is shown, but an increase of up to 0.1 often occurs when a rock is fractured. The velocity ratio is defined as the ratio of the compressional wave velocity (Vp) divided by the shear wave velocity (Vs). Poisson's ratio is defined as the ratio of the transverse contraction to the longitudinal extension of a rod subjected to an axial load. Poisson's ratio is also a qualitative measure of the amount of fracturing present in a rock mass. Therefore a map indicating variations of Poisson's ratio or the velocity ratio may indicate areas or volumes with anomalous fracturing and resultant high permeability.

Figure 16 is a plot of arrival time versus S-P times for eight events recorded by this survey. This relationship, often called the Wadati diagram method, has been discussed by others (Semyenov, A.N., 1969; Nersesov, et.al., 1971; Kisslinger, Engdahl, 1973). These eight events showed good S-wave breaks and were well recorded across the net. Figure 16 gives two values for each slope. The A parameter is the slope of the linear relationship which indirectly gives the velocity ratio and σ gives the corresponding Poisson's ratio from Figure 15.

Figure 17 is a plot of the velocity ratio with time. Variations from a constant velocity ratio have been used to study premonitory phenomena for large earthquakes with some

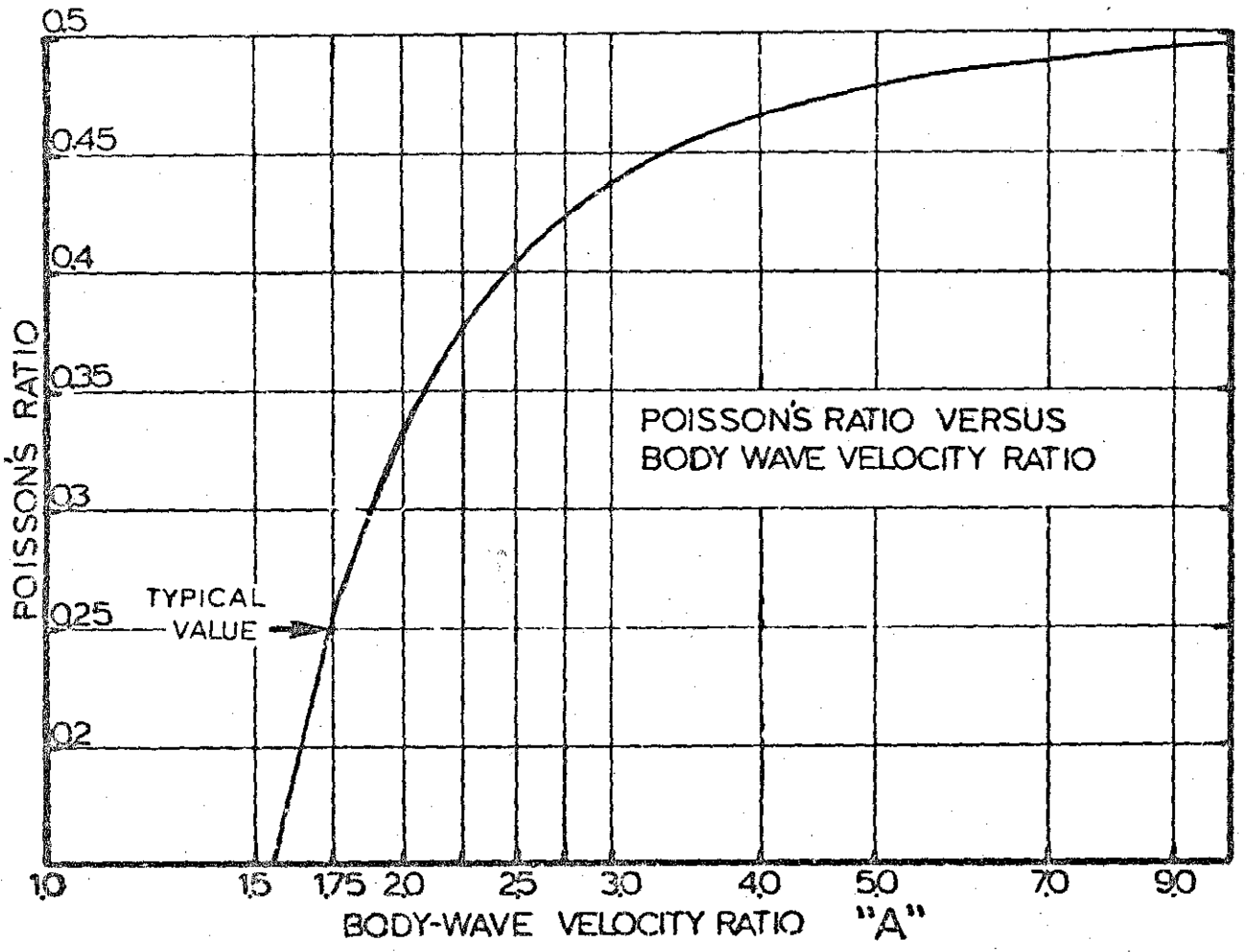

fig 15

THIS FIGURE SHOWS THE RELATIONSHIP BETWEEN POISSON'S RATIO AND VELOCITY RATIO. THE OFTEN ASSUMED VALUE OF 0.25 IS INDICATED.

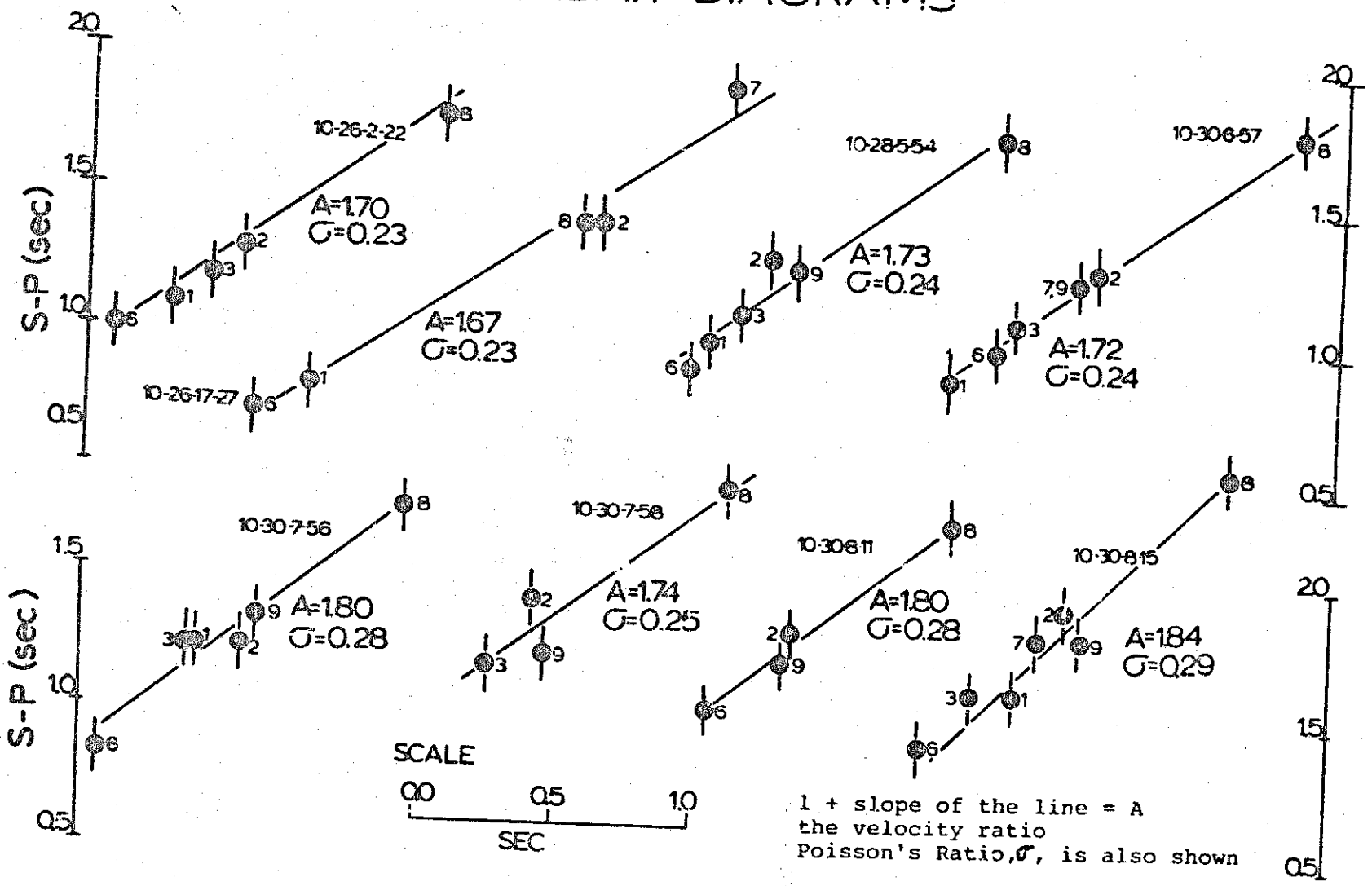

FIGURE 16

PLOT OF S-P TIME VERSUS P ARRIVAL TIME. EACH CURVE REPRESENTS A SEPARATE EVENT, EACH DATA POINT (IDENTIFIED BY STATION NUMBER) REPRESENTS AN INDIVIDUAL RECORDING OF THAT EVENT

success (Semyenov, 1969; Nersesov, 1971; Kisslinger,Engdahl,1974). The short time-sampling period of this survey precludes any prediction from this data but the spatial distribution of Poisson's ratio can be interpreted.

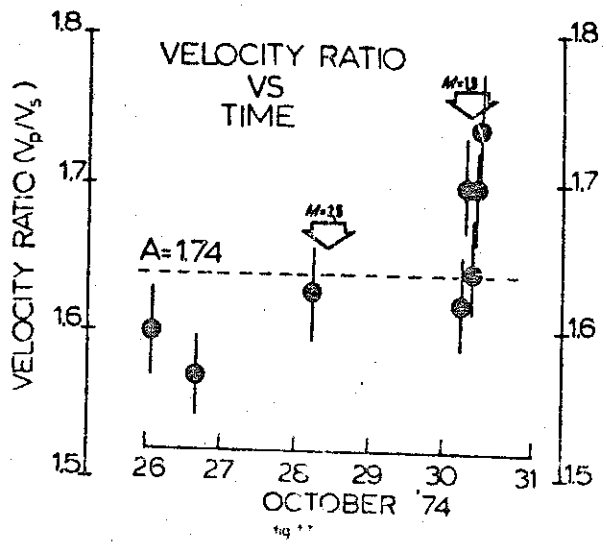

To locate an anomalously fractured zone, a map of the observed Poisson's ratio (plotted at the epicenter) was made (see Figure 18). Note that the form lines indicate trends in the data and are not contour lines. The Poisson's ratio was assumed to be more heavily influenced by the source region and mechanism than by the travel path, therefore the value was assigned to the epicenter. Assignment of the value to the travel path would complicate the display, but the same conclusion would be derived from the alternate display. Figure 18 produces a consistent picture of Poisson's ratio increasing to the west and with depth along the fault.

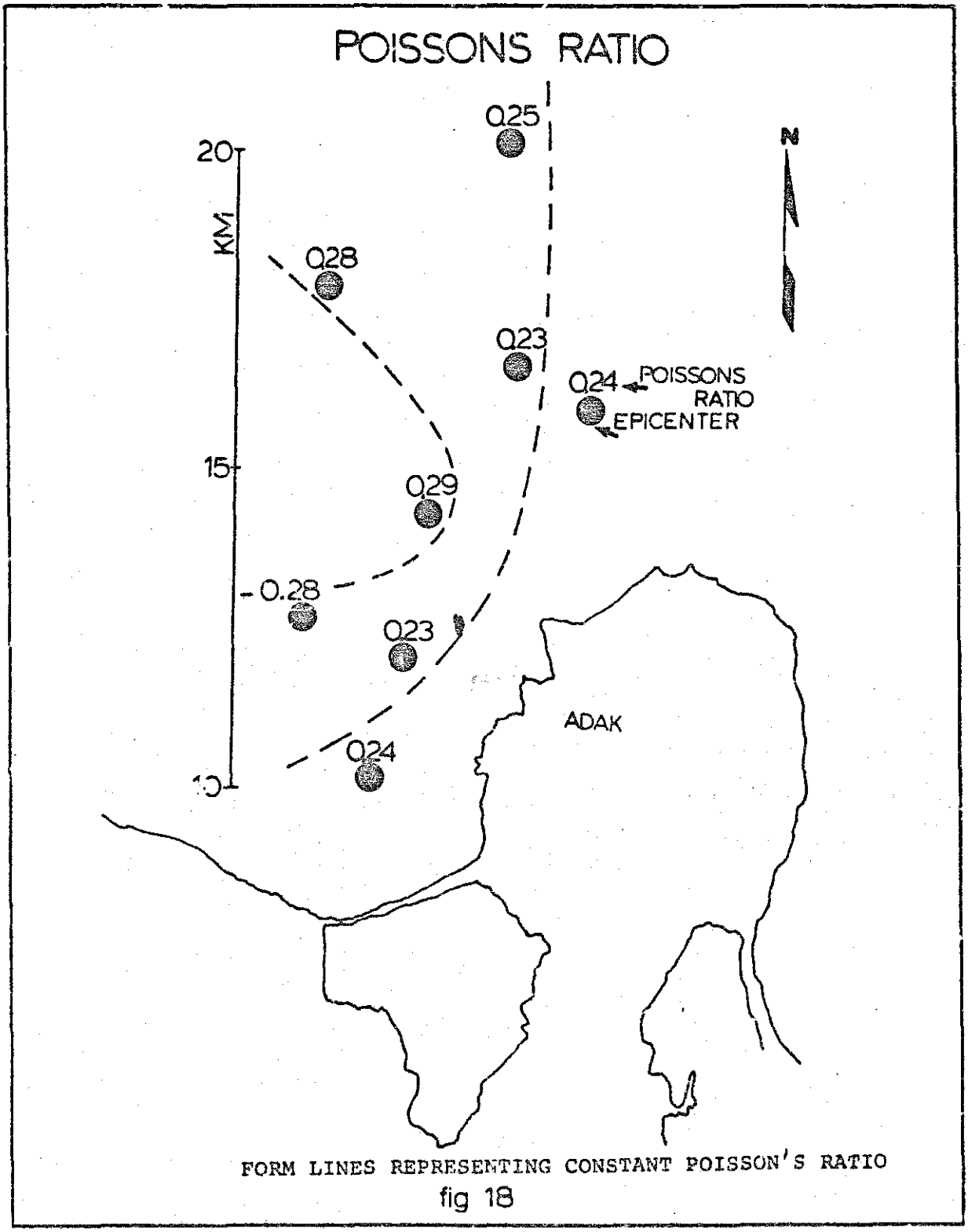

FORM LINES REPRESENTING CONSTANT POISSON'S RATIO

fig 18

The anomalous distribution of Poisson's ratio and its spatial relation to the geologic features can be explained by a theoretical model. This model is calculated by assuming a Volterra-type dislocation for the fault mechanism. For this model, the volume strain or dilation can be calculated around the fault given the spatial geometry of the fault plane. The Volterra-type dislocation model assumes that a homogeneous half-space is broken along a distinct plane and, after displacement, is welded back together. The half-space, which was initially stress free, now is subjected to a regional stress (manifested by the volume strain, which can be contoured) created by the dislocation at the "fault plane". The dilation or volume strain around such a dislocation model has been calculated by Yeatts (1975). Figure 19 shows a plan and cross section view of the dilation around a right-lateral, strike-slip fault dislocation.

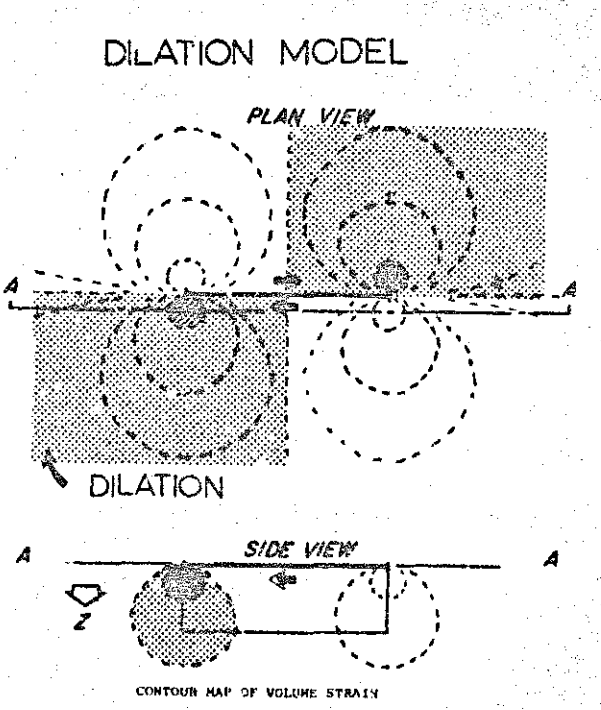

fig 19

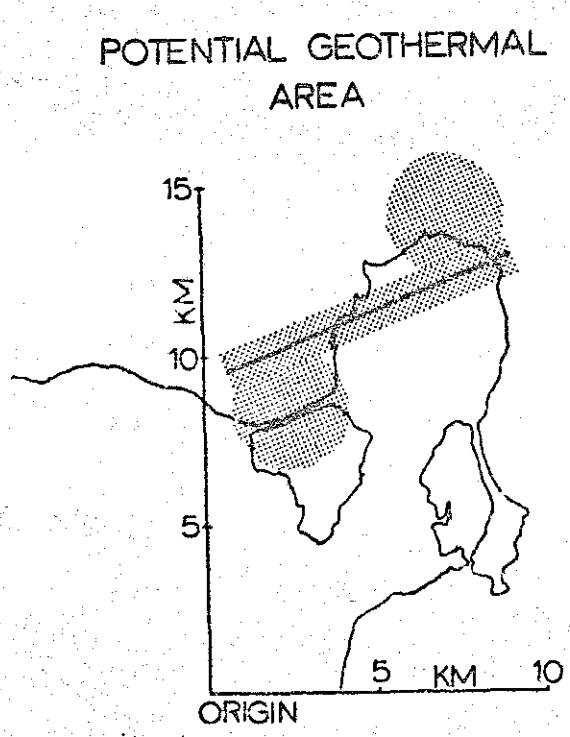

fig 20

The shaded areas represent areas under dilitation and unshaded areas are under compression. The region of most severe volume expansion can be expected to exhibit microfractures, demonstrated by ar increase in Poisson's ratio, leading to increased permeability.

Resistivity Survey

A resistivity survey was carried out in the Mount Adagdak peninsula area during the period October 25 to November 5, 1975, by a party under the supervision of Dr. Paul Donaldson of the Colorado School of Mines. The rotating dipole technique, as described by Tasci in Appendix A of this report, was used. Operations in the field on Adak in late Fall are frought with difficulties, largely induced by the cold, wet, and windy weather. Relatively few measurements were made before the survey had to be terminated, and the resistivity survey must be considered to be only preliminary in nature.

In the rotating dipole method, field data are obtained by making measurements of electric field intensity around a pair of bipole sources located at a single site, but with different orientations. For the Adak survey, a pair of sources, each 700 meters in length, was placed on the southwest slope of Mount Adagdak, as shown on the map in Figure 21. Currents of a few amperes were used to excite these two source bipoles. This is less than normally used in dipole mapping surveys, but only a small motor generator set was available for the survey, and grounding resistances were surprisingly high.

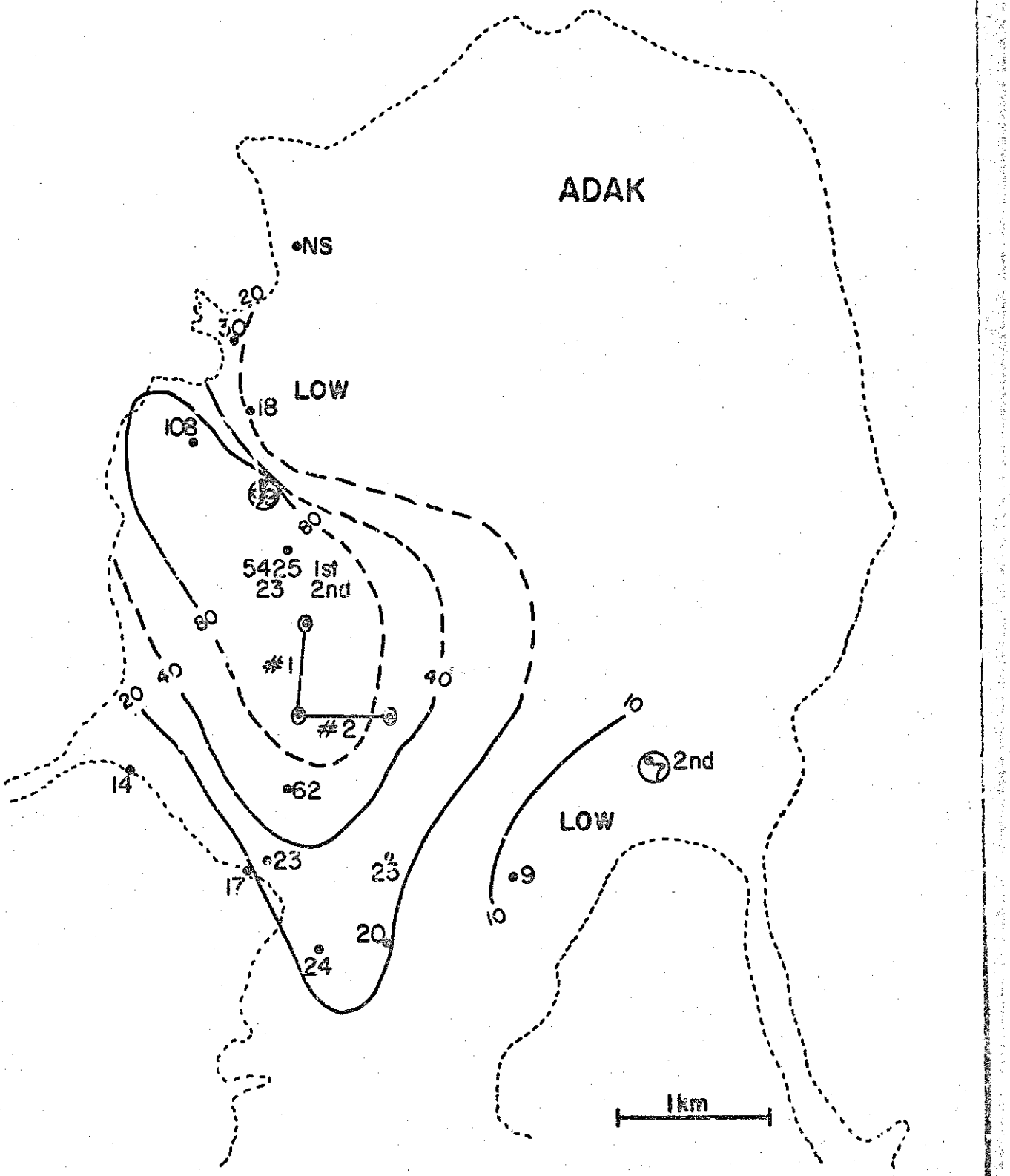

Figure 21. Apparent resistivities measured on Mount Adagdak in 1974.

Measurements were made at the receiver sites indicated on Figure 21, using receiver lines 100 meters in length. Voltages were recorded on paper-tape recorders. Values of apparent resistivity were computed for each source independently, and for various combinations of the two sources to yield resistivity values as a function of current flow directional at each receiver site. The maximum value of apparent resistivity is plotted and contoured on Figure 21, because this value is relatively immune to problems caused by false anomalies.

The roughly elliptical pattern of contours shown on this map, with high values of apparent resistivity being observed close to the source, is characteristic of an earth in which resistivity decreases with depth. It appears that at distances of less than 1 kilometer from the source, current has not penetrated deep enough to be controlled by the properties of rocks below sea level. At the greater distances, beyond 1 kilometer, apparent resistivity values decrease to less than 20 ohm-meters, or values which are compatible with the existence of geothermal fluids at depth. However, much more detailed coverage of the area will be required before the existence of any potential geothermal reservoir can be indicated.

Interpretation

A seismically active zone exists near Andrew Bay, north and west of Mount Adagdak on Adak Island, Aleutians Islands, Alaska. This zone is interpreted as a right-lateral, strike-slip fault with a small component of thrust. The surface trace of this fault should be apparent on the west side of Mount Adagdak.

A zone of relatively high Poisson's ratio mapped in this area indicates that a fractured or dilated region exists in the area. Consideration of the microearthquake station locations and the travel paths from the recorded events indicates the dilation zone probably exists south of and on the west end of the active fault zone.

Reconciliation of the theoretical model with the field observations also indicates that a dilated zone should be found north of and on the eastern end of the active fault plane. Due to the array geometry and location of the active seismic region, no data was obtained to confirm or deny the existance of this second anamolous zone.

Due to the increased permeability caused by the fracturing associated with the mechanism of faulting in the region, the hypothesized zones of volume expansion along the active trace of the fault are interpreted as having the highest potential of producing commercial earth steam. These areas are shown in Figure 20. The interpretation is of course, subject to clarification when reconciled with additional geological and geophysical data in the project area.

REFERENCES

Brune, J.N., and Allen, C.R., 1967, A microearthquake survey of the San Andreas Fault system in Southern California; BSSA, v.57, no.2, p.277-296.

Engdahl, E.R., 1973. Relocation of intermediate depth earthquakes in the central Aleutians by seismic ray tracing. Nature (Phys, Sci.), 245 (141): 23-25.

Kisslinger, C. and Engdahl, E.R., 1973. The interpretation of the Wadati diagram with relaxed assumptions. Bull. Seismol. Soc. Am.,63: 1723-1736.

Kisslinger, Carl and Engdahl, E.R., 1974. A test of the Semyenov prediction technique in the central Aleutian Islands. Tectonophysics, v.23, 237-246.

Glover, D., Personal communication.

Hamilton, R.M., and Muffler, L.J.P., 1972, Microearthquakes at the Geysers geothermal area, California: JGR, v.77, p2081-2086.

Lange, A.L., and Westphal, W.H., 1969, Microearthquakes near the Geysers, Sonoma County, California: JGR, v.74, p4377-4378

Nersesov, I.L., Semyenov, A.N. and Simbireva, I.G., 1971. Space-time distribution of the ratio of travel-times of compressional transverse waves in the Garm region. In: M.A. Sadovsky (Editor), Experimental Seismology. Nauka, Moscow, pp.334-348 (in Russian).

Semyenov, A.N., 1969. Variations in the travel-time of transverse and longitudinal waves before violent earthquakes. Izv. Acad. Sci. U.S.S.R.(Phys. Solid Earth), 4: 245-248 (English edition).

Ward, P.L., 1972, Microearthquakes: prospecting tool and possible hazard in the development of geothermal resources: Geothermics, v.1, no.1, p.3-12.

Ward, P.L., and Bjornsson, 1971, Microearthquakes, swarms, and the geothermal areas of Iceland: JGR, v.76, p.3953-3982.

Ward, P.L., and Jacob, K.H., 1971, Microearthquakes in the Ahuachapan geothermal field, El Salvador, Central America: Science, v.173, p.328-330.

Yeatts, - In press (1975)

END

DATE

FILMED

9-7